CARL VON OSSIETZKY universität OLDENBURG

Optimizing performance and understanding stability issues in polymer:fullerene solar cells

Von der Fakultät für Mathematik und Naturwissenschaften
der Carl von Ossietzky Universität Oldenburg
zur Erlangung des Grades und Titels eines
Doktors der Naturwissenschaften (Dr. rer. nat.)
angenommene Dissertation von

Antonietta De Sio

geboren am 17. Juni 1981
in Salerno, Italien

Erstgutachter: Prof.Dr. Jürgen Parisi (Universität Oldenburg)
Zweitgutachterin: Prof.Dr. Elizabeth von Hauff (Universität Freiburg)
Drittgutachter: Prof.Dr. Carsten Agert (NEXT ENERGY, Oldenburg)

Tag der Disputation: 24. April 2012

Contents

Abstract

In this thesis, different approaches will be pursued, in order to control the performance of polymer:fullerene solar cells. First, a brief introduction of the basic working principle of polymer solar cells and details on the sample preparation and the characterization methods are given. Next, molecular doping is proposed to tune the electronic properties of a novel low bandgap copolymer. The effect of doping in the corresponding polymer:fullerene solar cells will also be analyzed. The role of the active layer morphology in the reference P3HT:PCBM material system is investigated by exploring the influence of a combination of solvents with different boiling points on the optical, electrical and structural properties of the blend films and solar cells. The effect of the device architecture on the performance will be addressed. In particular, inverted devices containing no indium-tin-oxide, no water based buffer layers and no low work function metals will be fabricated and compared to the standard forward architecture. The effect of processing the devices in ambient air instead of in a nitrogen-filled glovebox as well as the degradation of the active layer induced by exposure to oxygen and light on the optoelectronic properties of the P3HT:PCBM model system will be investigated.

Kurzfassung

In dieser Arbeit werden verschiedene Ansätze verfolgt, um das Verhalten von Polymer:Fulleren Solarzellen zu beeinflussen. Zuerst wird eine kurze Beschreibung der grundlegenden Arbeitsprinzipien von Polymer-Solarzellen gegeben und Details der Probenherstellung und -Charakterisierung werden vorgestellt. Als nächstes wird molekulares Dotieren als Möglichkeit vorgeschlagen, die elektronischen Eigenschaften eines neuartigen low-bandgap-Copolymers zu modifizieren. Der Effekt dieser Dotierung in den zugehörigen Polymer:Fulleren-Solarzellen wird ebenfalls analysiert. Die Rolle der Morphologie der aktiven Schicht wird erforscht, indem der Einfluss der Verwendung einer Kombination von Lösungsmitteln mit unterschiedlichen Siedepunkten auf die optischen, elektrischen und strukturellen Eigenschaften eines P3HT:PCBM-Referenzsystems untersucht wird. Der Effekt der Architektur auf die Leistung der Zelle wird besprochen. Insbesondere werden invertierte Zellen unter Verzicht auf Indium-Zinn-Oxid, wasserbasierte Pufferschichten und Metalle mit niedrigen Austrittsarbeiten hergstellt und mit solchen basierend auf der Standardstruktur verglichen. Zuletzt wird der Einfluss sowohl der Herstellung der Zellen in Umgebungsluft statt in einer Glovebox unter Stickstoffatmosphre als auch der Degradation durch Sauerstoff und Licht auf die optoelektronischen Eigenschaften des P3HT:PCBM-Referenzsystems untersucht.

Chapter 1

Introduction

In this chapter, a brief overview of the fundamental processes regulating the photovoltaic action of the active materials as well as the operational principle of polymer solar cells is given.

1.1 Conjugated polymers

Conjugated polymers are a class of carbon based macromolecules that derive their semiconducting properties from having delocalized π-electron bonding along the polymer chain. The π bonding and π^* antibonding orbitals form delocalized wavefunctions, which support mobile charge carriers [1]. The filled π band is called the *highest occupied molecular orbital* (HOMO), while the empty π^* band is called the *lowest unoccupied molecular orbital* (LUMO). The energy difference between the HOMO and LUMO defines the bandgap and depends on the conjugation length [2]. Thus, disruption of the conjugation along the polymer backbone affects the local HOMO and LUMO positions, hence, the bandgap.

Absorption of a photon with appropriate energy promotes an electron from the filled π-band to the empty π^*-band, i.e., from the HOMO to the LUMO. This excitation creates a Coulomb bound hole-electron pair, called *exciton*. In a three-dimensional semiconductor, like, for example, crystalline silicon, the excitons are weakly bound due to the high dielectric constants and dissociate therefore into free electron-hole pairs. These are called Wannier excitons. Due to their strong intramolecular electronic interactions and relatively weak intermolecular electronic interactions, conjugated polymers behave as quasi-one-dimensional sys-

tems [3]. Spatial and energetic disorder leads to localization of the excitations [4] on small conjugated segments [5, 6]. Due to the localization and the low dielectric constants of polymers, the excited species are strongly bound electron-hole pairs similar to Frenkel excitons [7] in molecular crystals. Therefore the exciton is unlikely to separate at room temperature [8].

Moreover, the charge transport proceeds by hopping, i.e., inelastic tunneling between localized states [9], and the energy required to jump from one state to the other is provided by the interaction with phonons. Hence, in contrast to conduction by electrons in bands, like in a three-dimensional crystal, where the interaction with phonons reduces the mobility due to the increased lattice scattering [10], in disordered semiconductors such interactions stimulate hopping, and the mobility shows a positive trend with the temperature. The charge transport properties of conjugated polymers depend on the packing of the chains and the ordering in the solid films, as well as on the density of impurities and structural defects. Therefore, the mobility values of the same polymer show large variations, depending on the quality of the sample [11].

Conjugated polymers gained huge scientific interest in the last decades, because of their ability to combine the optoelectronic properties of the inorganic semiconductors and the technological advantages of the polymers [12], such as the possibility of fine tailoring of the optoelectronic properties by chemical manipulation and solution processing at low temperatures. Furthermore, they are characterized by high absorption coefficients of the order of $10^5\ cm^{-1}$ at the maximum of the absorption spectrum [13], making it possible to use a layer thickness at the nanometer scale. Conjugated polymers represent, therefore, a promising class of materials to develop flexible, light weight and low cost photovoltaic applications [14, 15].

1.2 Polymer:fullerene donor acceptor systems

Upon light absorption, an exciton is created on the polymer chain. The exciton has a low diffusion length, of the order of few tens of nanometers [16], therefore, it tends to recombine resulting in a relatively poor photocurrent. This is the reason why the early studied single layer cells based on a Schottky organic diode [17] are not interesting for applications. By providing an acceptor with higher electron affinity, like a fullerene, the dissociation of excitons created close

to the donor-acceptor interface is favored via *charge transfer* to the acceptor. However, only the excitons created within a distance lower than the diffusion length from a donor-acceptor interface will have the chance to reach the interface and separate into a free electron-hole pair. Once the exciton is dissociated, the electron and hole must be transported through the acceptor and donor paths to the respective electrodes, in order to be collected. For this to happen, well defined and continuous donor and acceptor paths are necessary.

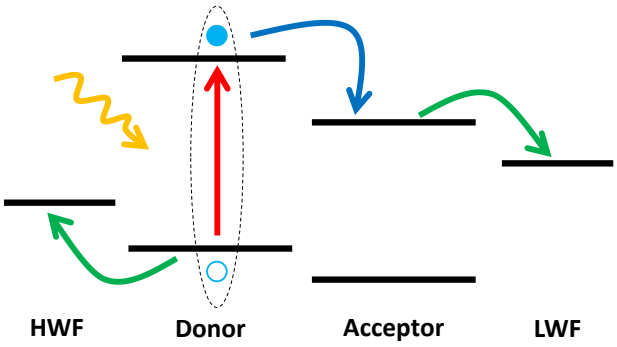

Figure 1.1: Sketch of the working principle of a donor-acceptor solar cell

Figure 1.1 depicts the operational principle of a donor-acceptor organic solar cell. The red vertical arrow indicates the formation of the exciton following light absorption, the blue arrow refers to the charge transfer process and, finally, the green arrows indicate the transport of electrons and holes towards the low work function (LWF) and high work function (HWF) electrodes respectively.

As the last step, the charge carriers have to be extracted through the contacts, in order to give rise to the photocurrent. Hence, ohmic contacts are needed. In general, at a semiconductor-metal interface, ohmic or rectifying contacts can be formed, depending on the relative position of the work function of the metal and the Fermi level of the semiconductor [18]. An ohmic contact for electron extraction, for example, is achieved if the work function of the metal is below the Fermi level of the semiconductor [18]. For polymer solar cell structures, it has been proposed that the formation of an ohmic contact for electrons is achieved when the LUMO of the acceptor is aligned with the Fermi level of the LWF electrode [19]. However, the work function alignment alone does not ensure efficient charge collection. The barrier height at the interface, the electrode geometry and interface quality are also important.

In polymer solar cells, it is common to use interlayers at both the anode and

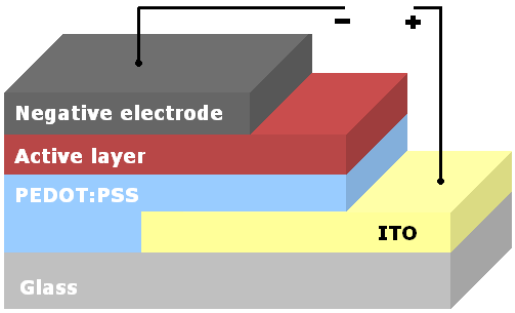

Figure 1.2: Typical device structure of a polymer:fullerene solar cell

the cathode, in order to improve the charge collection. It is, in fact, well established the use of a thin layer of *poly(3,4-ethylene-dioxythiophene):poly(styrenesulfonate)* (PEDOT:PSS) between the transparent conductive anode (HWF) and the active layer to enhance the hole collection, improve the electrode quality by minimizing shunts, and as electron blocking layer. At the cathode (LWF), the use of low workfunction materials such as Ca or LiF has been shown to improve the photovoltaic performance and, in particular, the photovoltage [20]. The typical structure of a polymer solar cell is shown in figure 1.2.

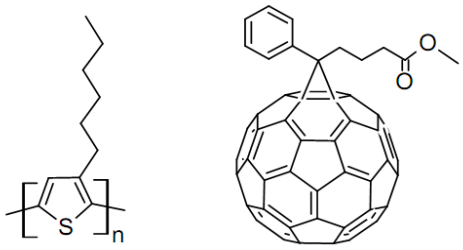

Figure 1.3: Chemical structure of P3HT (left) and PCBM (right)

The most widely reported active layer system in polymer solar cells consists of the conjugated polymer *poly(3-hexylthiophene)* (P3HT) as the donor and *[6,6]-phenyl-C61-butyric acid methyl ester* (PCBM), a soluble derivative of the fullerene C_{60}, as the acceptor. The chemical structures of these materials are shown in figure 1.3.

1.3 Photophysical processes

Exciton dissociation through photoinduced charge transfer is a fundamental step for efficient energy conversion of the incident light in polymer solar cells. In general, the excitons can decay, in a radiative or non-radiative way, or be dissociated in a free electron-hole pair via charge transfer to the acceptor [21]. Therefore, photoinduced charge transfer reduces the emission from the excited state in the donor by transferring the excited electron to the acceptor. However, reduction of the emission (luminescence) in a blend can also indicate other phenomena. In general, the decrease in the intensity of luminescence from a molecule due to the interaction with another material (the quencher) is called *quenching*. For quenching to occur, the emissive molecule and quencher must be in molecular contact so that their electron clouds can interact [22].

1.3.1 Luminescence quenching

There are different kinds of luminescence quenching. *Dynamic* or collisional quenching occurs when the luminescence of a material is reduced upon contact with the quencher and depends on their relative positions at the moment of the excitation. Therefore, the rate of collisional quenching in a thin film depends on the morphology. Another frequently observed quenching mechanism occurs when the quencher forms complexes with the emissive molecule in the ground state. This phenomenon is referred to as *static* quenching. Quenching of luminescence is formally described by the *Stern-Volmer equation*

$$\frac{PL_0}{PL} = 1 + K_{D,S}Q, \tag{1.1}$$

in which the ratio between the luminescence intensity in the absence (PL_0) and presence (PL) of the quencher is expressed as a function of the quencher concentration (Q) through the quenching constant (K_D in case of dynamic quenching or K_S for static quenching). In both cases, PL_0/PL is linearly dependent on Q. Therefore, quenching data obtained by steady-state photoluminescence measurements alone can be explained by dynamic or static processes. In order to distinguish them, time-resolved measurements are required. In fact, no change in the lifetime due to the presence of the quencher occurs in static quenching, because the observed luminescence from the non-complexed fraction of molecules is not affected, and the complexed one usually does not emit [22]. Another dif-

ference is that ground-state complex formation results in modifications of the absorption spectrum of the luminescent molecule, while for collisional quenching only the excited states are affected, and thus no changes in the absorption are expected upon contact with the quencher. In many cases, quenching is the result of both collisions and ground-state complex formation with the same quencher. The Stern-Volmer equation, in this case, results in a parabolic behavior with upwards curvature and can be expressed as follows:

$$\frac{PL_0}{PL} = (1 + K_D Q)(1 + K_S Q). \tag{1.2}$$

1.3.2 Photoinduced charge transfer

Photoinduced charge transfer is also a kind of luminescence quenching that involves a donor and an acceptor (figure 1.4).

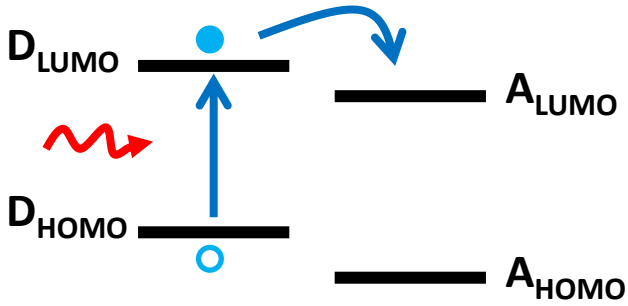

Figure 1.4: Scheme of photoinduced charge transfer between the donor and the acceptor

In this case, a complex between the donor and the acceptor is formed upon excitation of the donor yielding a negatively charged acceptor. Such complex may emit a photon or return to the ground state in a non-radiative way. In both cases, the total energy of the charge transfer complex decreases. It is important to note that the donor and the acceptor do not usually form a complex when both are in the ground state, because this is energetically unfavorable. The energy change for photoinduced charge transfer depends on the reduction potentials of donor and acceptor [22] through the equation

$$\Delta G = IP_D - EA_A - C(R), \tag{1.3}$$

where IP_D is the ionization potential of the donor, EA_A the electron affinity of the acceptor, and $C(R)$ the Coulomb potential energy of the electron-hole

pair. The energy of the charge transfer state is, therefore, lower than the energy before electron transfer. This charge transfer is reported to be extremely fast in conjugated polymers, on the order of tens of femtoseconds [21, 23, 24].

In polymer:fullerene blends, photoinduced charge transfer between the donor and the acceptor is a fundamental step for the operation of the solar cells.

1.3.3 Resonance energy transfer

Another process that can take place in the excited state between a donor and an acceptor is *resonance energy transfer*. This process manifests itself whenever the emission spectrum of the donor overlaps with the absorption spectrum of the acceptor, and the rate of energy transfer is determined by the distance between the donor and the acceptor over the Förster distance [25]. The latter is defined as the distance at which the energy transfer efficiency is 50% and is normally between 10 and 100 Å. A scheme of this process is shown in figure 1.5, where the yellow arrow represents the coupled transition between the acceptor and the donor.

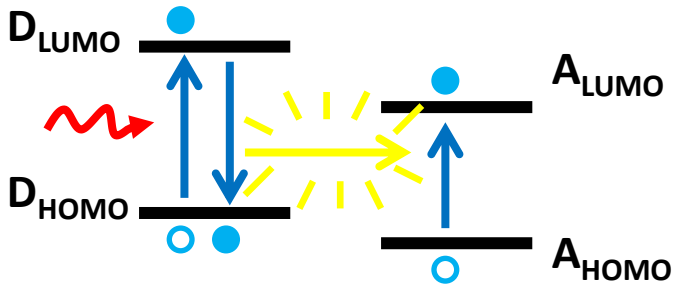

Figure 1.5: Scheme of resonance energy transfer between the donor and the acceptor

The energy of the photoexcited donor is transferred in a non-radiative way to the acceptor so that the latter results in the excited state while the donor excitation is reduced. Hole back transfer from the indirectly excited acceptor to the donor may take place. However, it is not clear how efficient this back transfer is compared to direct electron transfer [26]. In contrast to photoinduced charge transfer, resonance energy transfer does not require molecular contact between the donor and the acceptor. Furthermore, no direct electron transfer takes place, but instead, the excitation itself is transferred [3]. It represents, therefore, a loss channel for effective photovoltaic action of a donor-acceptor blend [27].

1.4 Bulk heterojunction concept

The first organic solar cell, consisting of a bilayer of donor and acceptor sandwiched between two electrodes, was reported in 1986 with efficiency slightly lower than 1% [28]. In the nineties, the introduction of the bulk-heterojunction concept [19] allowed to enhance the efficiency to about 3%, marking a breakthrough in the field of polymer photovoltaics. In this structure, the active layer consists of an intermixing of the donor and acceptor materials so that a fine interpenetrating network builds up with extended donor-acceptor interfaces distributed in the bulk. This tremendously increased the efficiency of charge separation with respect to the bilayer structure. Recently, the power conversion efficiency of these devices reached certified values above 8% [29], thank to the development of new low-bandgap polymers [30] that allow for increased light harvesting. A comparison between the bilayer and bulk heterojunction concept is represented in figure 1.6

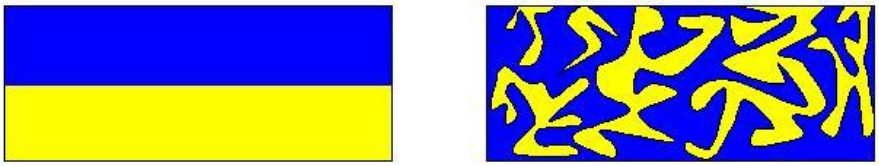

Figure 1.6: Schematic representation of bilayer (left) and bulk heterojunction (right) configuration

The enhanced performance with respect to the bilayer concept results from a bicontinuous network of internal donor-acceptor heterojunctions that makes it possible to improve the efficiency of charge separation and, therefore, the device efficiency [19]. In the bilayer solar cell, the active layer consists of a single donor-acceptor interface available for exciton dissociation. On the other hand, an interpenetrating network of donor and acceptor at the nanometric scale improves the charge separation rate, but at the same time introduces a new issue due to the fact that well defined donor and acceptor paths are required to achieve efficient transport. Since the interpenetrating network is made by mixing the donor and acceptor in solution, a defined connection between the donor domains towards the HWF electrode and the acceptor domains towards the LWF electrode is not guaranteed [31]. Achieving percolation of the two phases throughout the whole active layer is not trivial. In fact, the donor and acceptor domains should

be small enough so that the highest amount of photogenerated excitons can be dissociated and, at the same time, provide continuous percolating networks towards the respective electrodes to avoid transport related losses. It is therefore evident that, for an efficient bulk heterojunction solar cell, a good control of the morphology is important [32, 26].

1.4.1 The role of morphology

The morphology of the active layer is sensitive to the processing conditions, such as the donor to acceptor ratio [33], solvent [34, 35] and post-processing steps, like thermal annealing or solvent swelling [36, 37]. Several studies [32, 38, 39, 40, 41, 42, 43] have shown that the solvent has a strong influence on the film formation and can favor or inhibit a preferential phase segregation in the active layer. In the case of semicristalline polymers like *regioregular* (rr-) P3HT, the deposition conditions have a large impact on the ordering of the polymer and consequently alterate its optical and electrical properties. In P3HT:PCBM based bulk heterojunction solar cells, the crystallization of the polymer phase can be restrained by the clustering of the fullerene during drying [44]. Solvents with selective solubility for the fullerene can avoid this phenomenon by minimizing the fullerene clustering. The role of the casting solvent in the control of the morphology will be investigated in more detail in chapter 4.

1.5 Solar cell performance

The current-voltage characteristic of a solar cell can be described by the equation

$$I = I_s(e^{\frac{q(V-IR_s)}{nkT}} - 1) + \frac{V - IR_s}{R_p} - I_{ph}, \tag{1.4}$$

where I_s is the dark or reverse saturation current, n the ideality factor of the diode, R_s the series resistance, R_p the shunt resistance, and I_{ph} the photocurrent. The power conversion efficiency is the commonly used figure of merit for photovoltaic devices and is calculated as

$$\eta = \frac{J_{sc}V_{oc}FF}{P_{in}}, \tag{1.5}$$

where J_{sc} is the short circuit current density, V_{oc} the open circuit voltage, and FF the fill factor. An example of the current density-voltage (JV) characteristic of a sample polymer:fullerene solar cell is reported in figure 1.7.

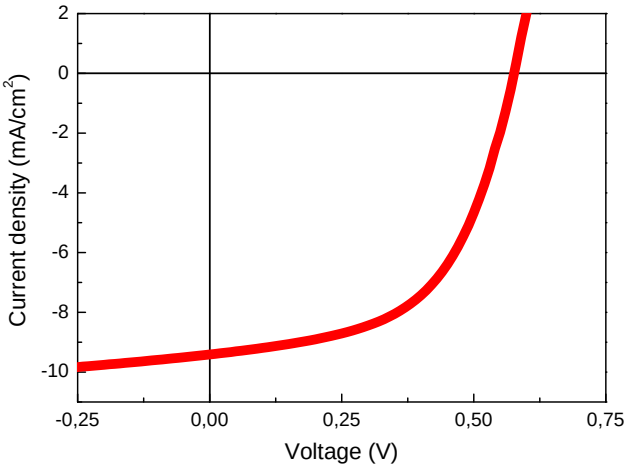

Figure 1.7: JV characteristic of a P3HT:PCBM solar cell

In bulk heterojunction solar cells, the photocurrent is determined by the amount of absorbed photons, the efficiency of exciton dissociation into free electrons and holes, the efficiency of charge transport and, finally, the efficiency of charge collection at the electrodes [45]. In a rough approximation, the current is a function of the optical properties of the active blend, in particular the absorption coefficient, and the morphology of the film. Therefore, in polymer solar cells, each detail of the realization process directly influences the performance of the final devices [46].

1.6 Stability

Another important aspect concerning polymer solar cells is the poor stability under operating conditions [47]. Most of the conjugated polymers degrade fast when exposed to ambient air and light. This is clearly one major drawback that needs to be overcome. The main focus of research is towards the improvement of the power conversion efficiency of the devices under simulated sunlight. The efficiency is certainly a major point, in order to compete with the more performant inorganic technologies like silicon based devices, but the stability, the production costs, and the processing are just as important [47, 48, 49]. These individual areas have received relatively less consideration. From the stability point of view, polymer based devices must be tremendously improved to become technologically interesting when compared to the 25 years stable silicon based solar cells for example. However, the degradation issue in polymer blends and devices is

rather complicated and not yet fully understood [50]. Indeed, estimations on the costs of production and device lifetime indicate that organic photovoltaics can be competitive with other technologies if a lifetime around 10 years is achieved [15, 14, 51].

1.7 Outline of the thesis

In order to control the performance of polymer:fullerene solar cells, different approaches will be pursued in this thesis. Details on the sample preparation and the characterization techniques used will be given in the second chapter. In the third chapter, molecular doping will be explored as a means to control the electronic properties of a low bandgap copolymer. Doping of the pristine copolymer via co-solution and the effect of doped active layers in the corresponding polymer:fullerene solar cells will be demonstrated. In the fourth chapter, the role of the morphology of the active layer in a P3HT:PCBM blend will be investigated by analyzing the effect of a combination of solvents with different boiling points on the optical, electrical, and structural properties of the blend and solar cells. In the fifth chapter, the effect of the device architecture on the performance will be probed. In particular, inverted device structures containing no indium-tin-oxide, no water based buffer layers, and no low work function metals will be fabricated and characterized. The effect of degradation due to processing the devices in ambient air as well as the irreversible degradation in the active layer induced by exposure to oxygen and light on the optoelectronic properties of the P3HT:PCBM model system will be investigated in the last chapter.

Chapter 2

Materials and methods

In this chapter, the details of the sample preparation as well as a brief description of the setups used for characterization are given.

2.1 Sample preparation

In this thesis, two kinds of polymers are investigated. In chapter 3, *poly[2,6-(4,4-bis-(2-ethylhexyl)-4H-cyclopenta[2,1-b;3,4-b']dithiophene)-alt-4,7-(2,1,3-benzothiadiazole)]* (PCPDTBT) is employed to demonstrate molecular doping via co-solution. PCPDTBT was supplied by Konarka Technologies GmbH (Germany). *Tetrafluoro-tetracyanoquinodimethane* (F4-TCNQ), from Sigma-Aldrich, was used as p-dopant. F4-TCNQ and PCPDTBT were separately dissolved in *chlorobenzene* (CB anhydrous 99.8% from Aldrich), in a concentration of 1 mg/mL and 10 mg/mL, respectively. A set of solar cells was prepared from chlorobenzene solutions obtained by blending the doped PCPDTBT with PCBM, purchased from Solenne BV, in a weight ratio of 1:1. For other blend solutions, PCBM was added to achieve a donor to acceptor ratio of 1:2 in weight, and diiodooctane 3% in volume was used as solvent additive to improve the performance. Doping concentrations between 0 and 0.3% and up to 1% were investigated. All the solutions were left stirring overnight at 80°C before deposition. The semiconducting layers were then spin coated in a nitrogen filled glovebox onto pre-cleaned substrates. Further details regarding the preparation procedure of the solar cells is reported in a following section.

In the remaining chapters, a reference system based on rr-P3HT is investi-

Solvent	Boiling point (°C)
oDCB	180
CB	130
THN	207

Table 2.1: Boiling point of the solvents used to dissolve the organic materials as reported on their datasheet

gated. P3HT, supplied by Merck Chemicals ltd UK in the framework of the BMBF Project "Entwicklung innovativer polymerer Solarzellen für Energieautonome Systeme" (EOS), and PCBM, purchased from Solenne BV, are blended 1:1 in weigth ratio. In chapter 4, the effect of the casting solvent is explored. *Ortho-dichlorobenzene* (oDCB) readily dissolves both P3HT and PCBM, therefore, it is chosen as the host solvent in the these experiments. CB and *tetrahydronaphthalene* (THN) are used as co-solvents. oDCB and CB are purchased from Aldrich, THN from Merck. Table 2.1 reports the boiling points of the investigated solvents. The mixed solutions consist of 10% in volume of the co-solvent and 90% of the host solvent, while the reference solution is prepared using the host solvent only. The solutions contain 20 mg/mL of P3HT, which corresponds to 1.5 wt% in the host solvent. The samples are deposited by spin coating the hot solutions in an inert environment.

In chapters 5 and 6, P3HT:PCBM solutions are prepared using only oDCB as solvent.

2.1.1 Solar cell preparation

Polymer:fullerene bulk heterojunction solar cells are prepared in two different configurations: forward and inverted. The forward devices are made with P3HT and PCPDTBT, the inverted ones only with P3HT.

To prepare the forward solar cells, ITO coated glass substrates, purchased from PGO (Germany), were partially etched in an HCl bath for 10 min, in order to define the anode area. The patterned substrates were then cleaned in acetone and isopropyl alcohol for 15 min and subsequently exposed to an oxygen plasma treatment for 10 min. A layer of PEDOT:PSS (Clevios P from H.C. Starck) was then spun on top of the ITO after passing through a 0.45 μm filter. The samples were subsequently dried by annealing at 180°C for 10 min. The thickness of the PEDOT:PSS layer was around 60 nm. Further processing steps were performed in

a nitrogen filled glove box. The active layer was spun on top of the PEDOT:PSS. When P3HT:PCBM was used, an annealing step at 150°C for 10 min was done before transferring the samples into the chamber of a thermal evaporator. The solar cells containing PCPDTBT as the active layer were not annealed. The cathode was formed by evaporating 20 nm of Ca and 130 nm of Al through a shadow mask at a rate of 0.1 nm/s. The film thickness was determined using a Veeco Dektak 6M stylus profiler. The active area of the devices ranged between 0.10 and 0.25 cm^2.

For the preparation of the inverted solar cells, sputtered ZnO:Al were used as substrate instead of ITO. A description of the preparation of the ZnO:Al substrates is given later. The substrates were first cleaned in isopropyl alcohol before being transferred to a nitrogen filled glovebox where the other processing steps were performed. The active layer, consisting of a blend of P3HT and PCBM, 1:1 in weight ratio, dissolved in oDCB at a concentration of 2wt%, was spun directly on top of the ZnO:Al to obtain films with a thickness of about 230 nm. The samples were then annealed at 150°C for 10 min. The anode was thermally evaporated through a shadow mask. The thickness of the evaporated layers was determined using a calibrated quartz crystal microbalance during evaporation. The active area of the devices was 0.56 cm^2. Solar cells in the standard forward configuration on commercial ITO substrates with the same active layer thickness and the same active area as the inverted cells were prepared as control devices as explained before. The layer sequence for the standard devices was glass/ITO/PEDOT:PSS/P3HT:PCBM/Ca/Al.

2.2 Characterization techniques

Optical, electrical and structural characterization was performed on thin films and complete devices. In this section, a short overview of the methods used is given.

UV-Vis spectrophotometry

The absorption spectrum of a semiconductor is important for its application in photovoltaic devices. The absorption spectra were calculated from the transmittance T and reflectance R of the thin films spun on glass. The T and R spectra of each sample were measured using a Varian Cary 5000 spectrophotome-

ter equipped with an integrating sphere available at the EWE Research Center Next Energy, Oldenburg.

Photoluminescence spectroscopy (PL)

PL spectroscopy is a contactless, nondestructive method to probe the electronic structure of a semiconductor. A laser is used to photoexcite the sample and the radiative relaxation (luminescence) is detected. The PL is collected with a series of mirrors focusing on the entrance slit of a monochromator, and the signal is recorded using a lock-in amplifier. Analysis of the intensity and spectral content of the PL is a direct measure of various important material properties and can help in the determination of the bandgap, the impurity levels, and the detection of defects. By employing time-resolved measurements, the recombination mechanisms can be investigated. In this thesis, steady-state PL is performed on thin films spun on sapphire or quartz. PL spectra are recorded at low and room temperature in vacuum. The samples are mounted in a cryostat and are excited with lasers at 532 nm or 660 nm, depending on the bandgap of the material. The laser beam is directed on the sample through the sapphire windows of the cryostat.

Photoinduced absorption spectroscopy (PIA)

PIA is a kind of pump-probe spectroscopy, because it employs a pump beam, usually a laser, to excite the sample and a probe beam (a halogen lamp for example) to monitor the excited population. From the previous discussion in section 1.3 it is evident that the observation of PL quenching, upon mixing a polymer with a fullerene for example, is only an indirect method of detecting charge transfer between the donor and the acceptor. To directly investigate photoinduced charge transfer in a blend, PIA spectroscopy is a more accurate and reliable technique. A scheme of the PIA setup used for the investigation is shown in figure 2.1.

The sample is mounted in a cryostat with sapphire windows that allows to control the atmosphere during the measurements. A halogen lamp is used as the probe beam, while a laser is used as the pump. As in the case of the PL measurements, lasers at 532 nm or 660 nm are used for P3HT based samples and for PCPDTBT based ones, respectively. Furthermore, measurements at room temperature as well as at 80K are performed. In order to get the PIA spectrum

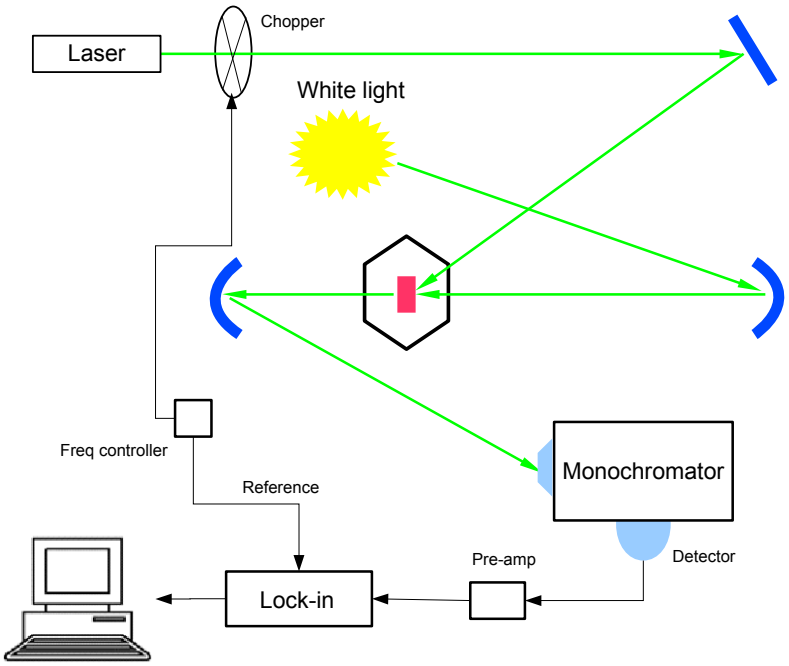

Figure 2.1: Scheme of the setup used for the PIA measurements

of a sample, three measurements are needed, i.e., the transmittance T of the whole system when illuminating the sample with white light only, the PL of the sample at the wavelength of interest and, finally, the transmission measured with both the laser and the white light on PA. The variation in the transmission is then calculated as follows:

$$-\frac{\Delta T}{T} = -\frac{PA - PL}{T}. \tag{2.1}$$

A plot of $-\frac{\Delta T}{T}$ as a function of the energy or wavelength is referred to as the photoinduced absorption spectrum of the sample. Negative signals indicate an increase in the transmitted probe light and can originate from ground state bleaching (GBS), corresponding to the depletion of the ground state population due to the excitation, or stimulated emission (SE), corresponding to an increased transmittance in the photoluminescence region [31]. Positive signals (PA) are due to a decrease in the transmitted light and originate from absorption of species towards higher excited levels [31], as shown schematically in figure 2.2.

Depending on the frequency modulation of the pump beam, it is possible to

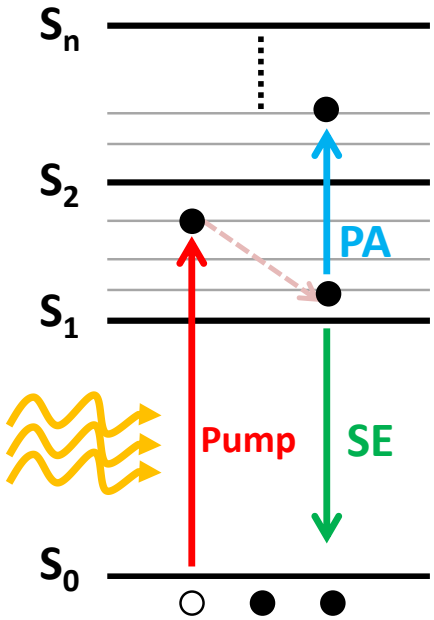

Figure 2.2: Principle of PIA spectroscopy

study the dynamics of the excited species at different time scales. In other words, different excited species are accessible by varying the chopping frequency. In this thesis, quasi-steady-state PIA will be used to characterize long-lived excitations in different conjugated polymers and polymer:fullerene blends. The frequency modulation of the pump excitation is 80 Hz and results in the observation of processes on a millisecond time scale.

Field-effect mobility measurements

Organic field effect transistors (OFETs) are the building blocks of more complex organic electronic devices. In material science, OFETs also represent a valuable and reliable tool for investigating the transport properties in organic semiconductors [52]. In fact, field effect mobility can be easily extracted by the output current-voltage characteristic. However, when comparing the charge transport properties of a semiconductor in an OFET structure with that of the relative solar cells, one has to take into account the different geometry and principle of operation of the two devices.

OFETs are here fabricated on highly n-doped silicon substrates purchased from Fraunhofer Institute for Photonic Microsystems (IPMS) in Dresden, with a thermally grown 230±10 nm thick SiO_2 layer. The electrical characterization is

carried out in a cryostat at 1×10^{-6} mbar in the dark. The output (source-drain) current-voltage characteristics are recorded using a Keithley 236 source measurement unit, while the gate voltage is regulated with a Keithley 2400 source measurement unit. OFET preparation and characterization were performed by Ali Veysel Tunc (Energy and Semiconductor Research Laboratory, Uni Oldenburg).

Charge extraction by linearly increasing voltage (CELIV)

CELIV allows to study the steady state transport properties in the same device architecture of the solar cells. A linearly increasing voltage pulse V(t) is applied to the device in reverse bias to extract the equilibrium charge carriers.

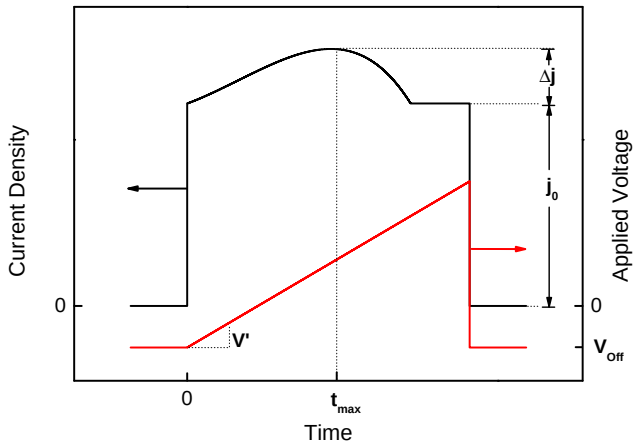

Figure 2.3: Applied voltage pulse (red) and current transient (black) used to extract the mobility

This leads to a typical current transient (as shown in figure 2.3) which can be used to calculate the mobility μ of the faster charge carriers [53] as

$$\mu = \chi \frac{2d^2}{V' t_{max}^2}, \tag{2.2}$$

where χ is a fitting parameter that depends on the relative height of the current transient $\frac{\Delta j}{j_0}$.

CELIV measurements are here performed on the solar cell structures in the dark under vacuum (10^{-6} mbar). A voltage pulse is applied to the device in reverse bias to avoid charge injection. The current response is measured using a DPO7104 oscilloscope from Tektronix. CELIV measurements were carried out by Ralph Huber (Energy and Semiconductor Research Laboratory, Uni Oldenburg).

Photovoltaic performance

The JV characteristics of the photovoltaic devices under illumination are measured with a Keithley 4200 semiconductor characterization system. The standard reference spectrum AM 1.5G is provided by a SS100AAA class A solar simulator from P.E.T. Inc. A reference silicon solar cell, from Fraunhofer Institute for Solar Energy Systems (ISE) in Freiburg, is used to calibrate the light. The efficiency is calculated according to the equation (1.5).

External quantum efficiency (EQE) spectra of the solar cells are also measured. EQE gives information on the spectral response of the device. The solar cell is illuminated with monochromatic light and the resulting photocurrent is measured. EQE is, therefore, defined as the ratio of the number of collected electrons divided by the amount of incident photons for each wavelength of interest

$$EQE = \frac{I_{sc}}{P_0}\frac{hc}{\lambda q}, \tag{2.3}$$

where P_0 is the incident optical power, h the Planck's constant, c the speed of light in vacuum, and λ the wavelength of interest.

In this work, EQE is measured with a Xe-Hg tandem lamp as the light source and a 2 grating monochromator to scan the wavelength. A calibrated silicon photodetector is employed to monitor the incident photon flux, while a lock-in amplifier is used to measure the photocurrent of the sample.

Transmission electron microscopy (TEM)

TEM is a kind of electron microscopy. It exploits the interaction between an electron beam transmitted through a thin film sample and the sample itself to build images. In this work, TEM is used to get insights into the morphology of the active layer. The semiconducting solutions are deposited on PEDOT:PSS coated ITO substrates, as described above. Free standing films are then obtained using the floatation technique. The samples are placed in deionized water (18.2 MΩ/cm) in a Petri dish and the free floating films are collected using suitable copper grids. All measurements are performed with a JEOL JEM-1011 transmission electron microscope operated at 100 kV. TEM images of the P3HT:PCBM samples were taken by Shany Neyshtadt, whereas the ones of the doped PCPDTBT:PCBM samples by Daniel Riedel (both at the Ludwig-Maximilians-Universität München).

Atomic force microscopy (AFM) and Kelvin probe force microscopy (KPFM)

AFM allows to obtain topographic images of a surface. A cantilever terminating in a sharp tip is used to scan the surface of the sample. When the tip approaches the surface of the sample, forces between the tip and the sample lead to a deflection of the cantilever. Typically, the deflection is measured using a laser spot reflected from the top surface of the cantilever into an array of photodiodes.

KPFM is a recently developed technique based on AFM. It allows to obtain both topographic and potential images. The potential is obtained by detecting the deflection of the cantilever caused by an electrostatic force between the tip and the sample. The contact potential difference between the tip and the sample is measured. This corresponds to the work function difference between the tip and the sample.

AFM and KPFM measurements of the P3HT:PCBM samples with various solvents are here performed with a UHV-STM/AFM system from Omicron at a pressure below 5×10^{-10} mbar to avoid the effects of oxygen and humidity on the surface of the sample. Pt/Ir cantilevers are calibrated using a gold single crystal as reference. The lateral resolution of the microscope in KPFM mode is 20 nm. AFM and KPFM measurements were done by Thomas Madena (Energy and Semiconductor Research Laboratory, Uni Oldenburg).

2.3 ZnO:Al preparation and characterization

ZnO:Al thin films were deposited onto pre-cleaned Corning®glass substrates by dc-magnetron sputtering. ZnO ceramic targets containing 2 wt% Al_2O_3 were used. The temperature of the substrates during deposition was 400°C. The thickness of the layers was determined with a Veeco Dektak 150 profilometer. A four point probing bridge from Jandel Engineering was used to measure the sheet resistance, while UV-VIS optical characterizations were performed with a Varian Cary 5000 spectrophotometer equipped with an integrating sphere. The surface roughness of the films was measured with a Nanosurf Mobile S atomic force microscope. The composition of the ZnO:Al films after deposition was analyzed by energy dispersed X-ray spectroscopy (EDX), using an X-Max silicon drift detector from Oxford Instruments. ITO substrates, purchased from PGO (Germany), were also characterized in the same way. The ZnO:Al thin films were fabricated

and characterized by Kambulakwao Chakanga (EWE Research Center Next Energy, Oldenburg).

2.4 Degradation experiments

In the last chapter, the effect of degradation on the reference P3HT:PCBM system is investigated. In the first part, the influence of the processing atmosphere is studied on the solar cells as well as on the active layer only by means of optical techniques. For the latter, rr-P3HT dissolved in oDCB is spun on sapphire substrates from hot solutions and annealed at 150°C for 10 min as for the solar cells. Absorption, PL and PIA spectra of the samples are measured. The corresponding solar cells in the forward structure are fabricated and characterized according to the procedure already explained in section 2.1.1. Reference samples are prepared entirely in a nitrogen filled glovebox, while the samples for the investigations of the effect of the processing atmosphere are prepared by spinning and annealing the active layer in ambient air.

In the second part of chapter 6, the effect of the irreversible degradation induced from light irradiation in presence of oxygen is investigated. The samples for these experiments are provided by Konarka Technologies GmbH, Nürnberg. Thin blend films are obtained by doctor-blading onto pre-cleaned glass substrates. The samples are annealed at 140°C in the glovebox for 2 min and then degraded under AM 1.5G light while kept in synthetic air. In order to remove the reversible component, the samples are annealed in the glovebox at 130°C for 10 min after the degradation and before being encapsulated. The samples are then sealed using a glass slab on top of the films and epoxy resin. PL and PIA measurements are performed with the setup described in the previous sections. Due to the epoxy resin, it is not possible to work at low temperature, therefore, the experiments are carried out at room temperature while keeping the samples under dynamic vacuum.

Chapter 3

Molecular doping

Doping of semiconductors using impurities with appropriate electronic properties is a general concept that does not depend on the nature of the semiconductor, but is common to both inorganic and organic materials. The ability to fine tune the electrical properties of a semiconductor by controlling the type and the concentration of the charge carriers with doping is one of the key techniques to develop efficient optoelectronic devices. For what deals with organic electronics, the discovery in 1977 that p-doping in polyacetylene dramatically increases its conductivity [54] boosted the research in this relatively new field and opened the way for the development of organic optoelectronic devices, like light emitting diodes and solar cells.

In small molecule based devices, prepared by evaporation of the organic precursors, the introduction of doped transport layers led to a reduced operating voltage [55] in organic light emitting diodes and allowed efficient p-i-n solar cells [56]. In such devices, the main contribution of doping is the modification of the energy barriers at the metal-organic interfaces which are well known to have a strong impact on the carrier injection and extraction efficiency [57, 58].

On the other hand, studies on conjugated polymer thin films demonstrated that molecular doping can lead to an increase in the conductivity and the mobility [59, 60]. In particular, it has been shown that doping affects the mobility in MEH-PPV [59], MDMO-PPV and P3HT [61] polymer films. Higher mobility due to controlled doping was demonstrated in both polymer diodes and field effect transistors [60]. However, the effect of molecular doping in polymer based solar

cells has not been investigated up to now. Therefore, in this chapter molecular doping will be explored in both polymer layers and bulk heterojunction solar cell devices based on a novel low bandgap copolymer. Part of the results presented here are adapted from A.V. Tunc, A. De Sio, D. Riedel, F. Deschler, E. Da Como, J. Parisi, E. von Hauff, *Molecular doping of polymer:fullerene solar cells: effects on transport and solar cells*, Organic Electronics 13, 290-296, 2012.

3.1 Low bandgap copolymers for increased light harvesting

Conjugated low bandgap polymers are able to absorb light in the near infrared range of the spectrum enhancing therefore light harvesting [62]. It is thus not surprising that design, synthesis and application of such novel materials are nowadays one of the hot topics in polymer photovoltaics [63, 64, 65].

PCPDTBT is a low bandgap copolymer based on two alternating repeat units, namely dithiophene and benzothiadiazole [66], and has an optical bandgap of about 1.45 eV. The chemical structure of PCPDTBT is shown in figure 3.1.

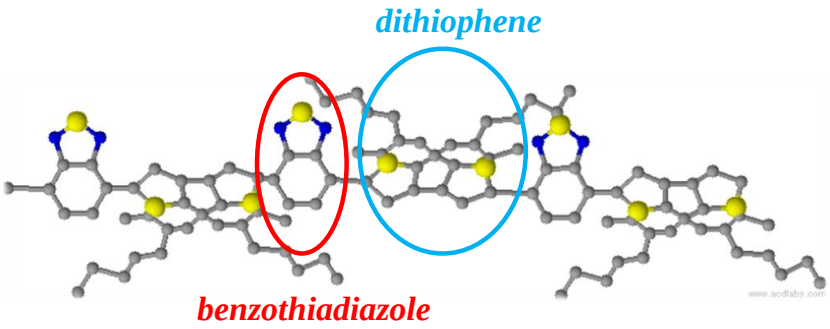

Figure 3.1: Chemical structure of the low bandgap copolymer PCPDTBT with indication of the repeat units: benzothiadiazole in red and dithiophene in blue

Figure 3.2 shows the normalized absorbance of PCPDTBT (red) and the one of P3HT (green) for comparison. While P3HT is essentially characterized by one broad absorption band peaking at 500 nm and more or less pronounced side shoulders depending on the ordering of the thin film, PCPDTBT has two main features, one smaller band centered at around 410 nm and a broader one at 720 nm. It is evident that PCPDTBT can absorb a higher amount of the incident

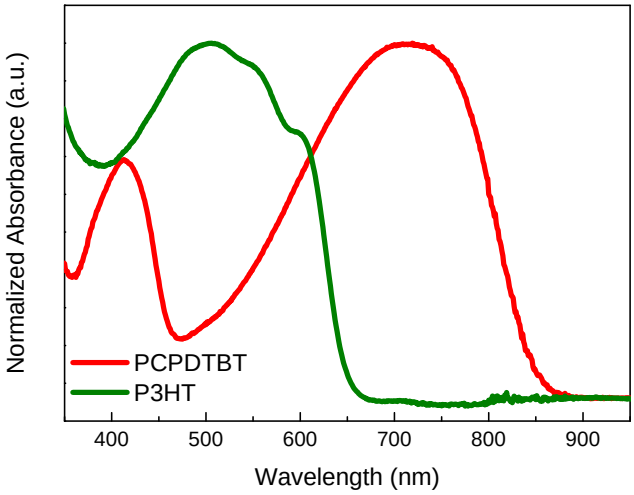

Figure 3.2: Normalized absorbance of PCPDTBT (red) and P3HT (green)

light with respect to P3HT and has, therefore, the potential to deliver a higher photocurrent in the corresponding solar cells.

Although, from the optical point of view, the blends of PCPDTBT and PCBM are promising for polymer photovoltaics [67], the charge transport properties are quite poor, and recombination limited devices are often obtained [68]. The use of solvent additives, like for example thiols [41], significantly improves the solar cell performance. However, poor charge transport and recombination losses still remain an issue and prevent full exploitation of the copolymer characteristics.

3.2 Molecular doping of PCPDTBT

F4-TCNQ is an organic molecule with a strong electron accepting character and can be deposited easily for the fabrication of electronic devices [69]. It has been widely used in organic light-emitting diodes to reduce the hole injection barrier, thereby improving the device performance [55, 70], as well as to efficiently p-dope graphene layers [71] and some conjugated polymers [59, 61]. Here, F4-TCNQ will be used as dopant for PCPDTBT. The effect of molecular doping on the optical, electrical and photovoltaic properties of PCPDTBT thin film will be investigated. Samples containing PCPDTBT doped with F4-TCNQ at concentrations between 0 and 1% were prepared as reported in section 2.1.

Figure 3.3 shows the normalized absorbance of PCPDTBT doped with F4-TCNQ at different concentrations. It can be seen that the absorption maximum

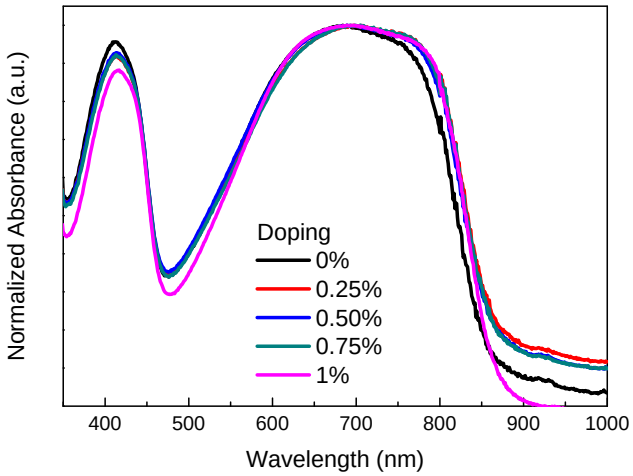

Figure 3.3: Normalized absorbance of PCPDTBT layers for different doping concentrations

slightly red shifts upon doping. The absorption in the high wavelength part of the spectrum, beyond 850 nm where the polymer itself no longer absorbs, also increases with the doping.

Figure 3.4 shows the PL spectra of the doped PCPDTBT layers. The data is corrected for the optical density of each film at the excitation wavelength (660 nm), in order to get rid of the difference in the thickness.

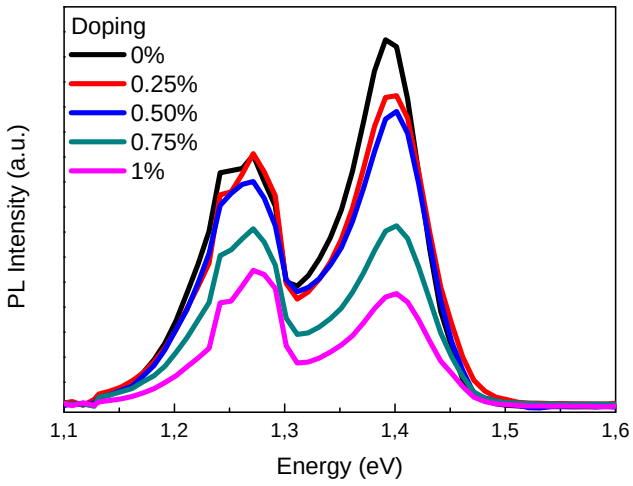

Figure 3.4: PL spectra of PCPDTBT layers for different doping concentrations

The PL intensity is visibly quenched when F4-TCNQ is added, in agreement with [72], and the quenching is enhanced with increased doping concentration. To further analyze the meaning of the PL quenching upon doping, the integrated

PL difference is shown in figure 3.5 in a Stern-Volmer plot. PL_0 indicates the integrated PL of the reference (undoped) sample, while PL is the one of the doped samples. The non-linear behavior with upwards curvature of the PL_0/PL with respect to the doping concentration indicates a combined dynamic and static quenching (see section 1.3). This means that F4-TCNQ and PCPDTBT are in molecular contact. Static quenching means that ground-state complexes between the polymer and the F4-TCNQ are formed upon doping. Moreover, the occurrence of static quenching is confirmed by the slight increase in the sub-bandgap absorption [22], seen in figure 3.3.

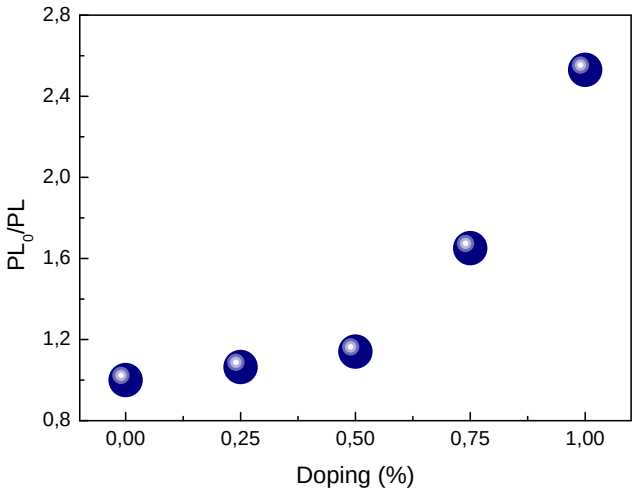

Figure 3.5: Stern-Volmer plot of doped PCPDTBT layers

The influence of the doping on the charge transport properties of PCPDTBT was investigated with field effect measurements. PCPDTBT was doped with F4-TCNQ at low concentrations, namely 0, 0.1, 0.2 and 0.3% in weight. Figure 3.6 reports the field effect hole mobility (μ_h) as a function of the doping concentration for the PCPDTBT (in blue) and for the blend with PCBM (in red, discussed in the next section).

From figure 3.6, it can be seen that the mobility increases with doping. In particular, the 0.3 % doped sample shows μ_h five times higher than the undoped one. The improvement in μ_h is significant at 0.1 %, and then only slightly increases up to 0.3 %. The source-drain current also increases with doping, as a result of the increase in the conductivity of the polymer (not shown here) [73]. This is consistent with results from literature demonstrating improved hole mobility for P3HT doped with F4-TCNQ [74]. The results of the charge transport

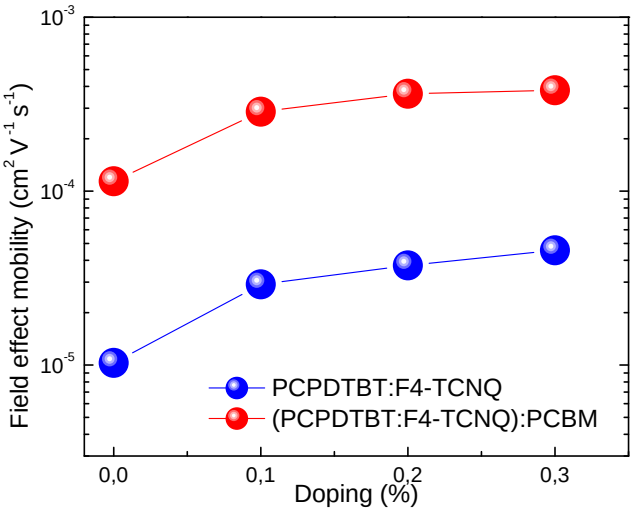

Figure 3.6: Field effect hole mobility of the PCPDTBT (blue) doped at low doping concentrations and its blend with PCBM (red) [measurements done by A.V. Tunc at the Universität Oldenburg]

investigations, together with the optical characterization (PL quenching), show that F4-TCNQ is able to p-dope PCPDTBT.

3.3 Effect of molecular doping in PCPDTBT:PCBM blends

In order to understand the behavior of the doped PCPDTBT in the photovoltaic devices, blends with PCBM were also investigated. Figure 3.7 shows the normalized optical density of doped PCPDTBT blended with PCBM as a function of the wavelength. It has been observed that blending PCPDTBT with PCBM leads to a blue shift of the absorption spectrum, resulting from a loss of molecular order in the copolymer phase due to the PCBM [75]. The use of solvent additives in the blend solution causes red shifting, indicating that the ordering has been restored [76]. Here, diiodooctane was used as solvent additive, therefore the absorption maximum shifts to about 800 nm.

The influence of the doping on the charge transport properties of the blends was also investigated with field effect measurements. The hole mobility as a function of the doping concentration is shown in figure 3.6 in red for the blends. The mobility is enhanced by a factor of three in the 0.3 % doped PCPDTBT blend with PCBM. As in the case of neat PCPDTBT (blue dots), the signif-

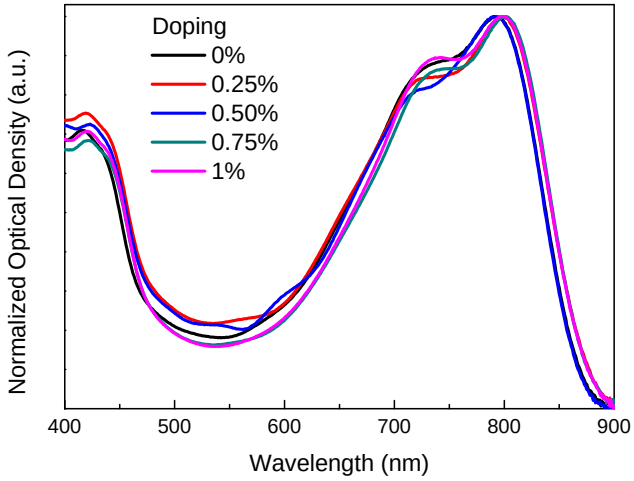

Figure 3.7: Normalized optical density versus wavelength of doped PCPDTBT:PCBM layers

icant enhancement is observed between 0 and 0.1 %, hence, at extremely low doping concentration. In the blends, between 0.2 % and 0.3 %, the mobility even seems to saturate, therefore, a higher concentration was not taken into account for charge transport investigations. The overall values are higher than in the case of PCPDTBT (blue dots), also for the undoped sample. This can be attributed to a different arrangement of the copolymer due to the introduction of PCBM. Improvement of the hole mobility with addition of fullerene to the polymer matrix is usually observed in PPV-based polymers [77]. These results clearly indicate that molecular doping can increase the hole mobility in PCPDTBT and PCPDTBT:PCBM blends. Improvements in the hole mobility of both the polymer and its blend with PCBM are expected to have an impact on the photocurrent of bulk heterojunction solar cells [77].

The influence of molecular doping on the excited states in blends of PCPDTBT and PCBM was investigated with steady-state PIA spectroscopy. Figure 3.8 shows the PIA spectra of the blends, for a doping concentration varying from 0 to 1%, normalized to the ground state bleaching (GSB), in order to account for the number of absorbed photons from the sample at the pump wavelength (660 nm). The PIA spectrum of the reference blend (black curve) is consistent with results from literature [78], where the peaks at 0.93 eV and 1.42 eV are assigned to polaron transitions. At 0.93 eV, the blend with 0.5% doping (blue curve in figure 3.8) shows the highest intensity in the polaron signal, while at 1.42

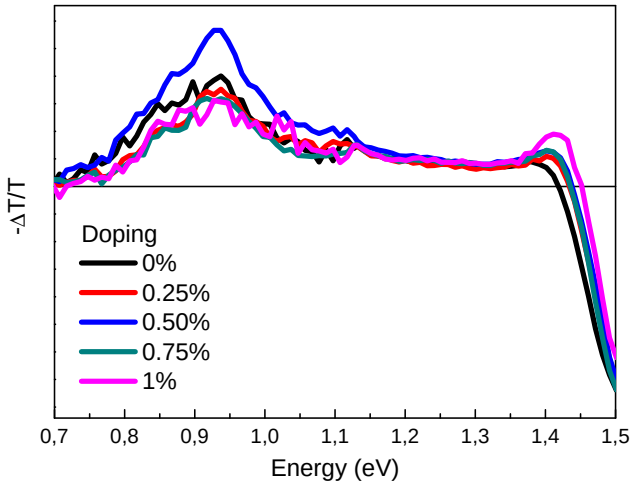

Figure 3.8: Steady-state PIA spectra of doped PCPDTBT:PCBM layers

eV a slight positive correlation with the doping concentration is observed. The intensity of the polaron peaks in the PIA spectrum can be directly correlated to the polaron density. The GSB onset at around 1.45 eV slightly shifts to higher energy with increasing doping concentration. This indicates that the tail states of the polymer are filled with the additional charge carriers from the F4-TCNQ, which shifts the emissive recombination of carriers to higher energy [72]. This also serves to explain the measured increase in the hole mobility upon doping.

In order to verify the role of the layer morphology, TEM images of the blends were also recorded. Figure 3.9 shows the TEM images of four doped blends. It is possible to distinguish fullerene and polymer domains from their brightness in the picture. In fact, PCBM domains appear as darker regions, while polymer ones are brighter. Figure 3.9 clearly shows PCBM domains with average in-plane dimensions of about 100 nm and irregular shape. The TEM images are similar so that it is possible to exclude morphology related effects in the mobility and polaron density enhancements. In other words, TEM confirms that the trend seen in the hole mobility and polaron density with doping does not result from changes in the film morphology due to the presence of the dopant.

3.3.1 Bulk heterojunction solar cells with molecularly doped active layers

Different bulk heterojunction solar cells containing blends of doped PCPDTBT and PCBM were fabricated and characterized (see section 2.1.1 for details). In

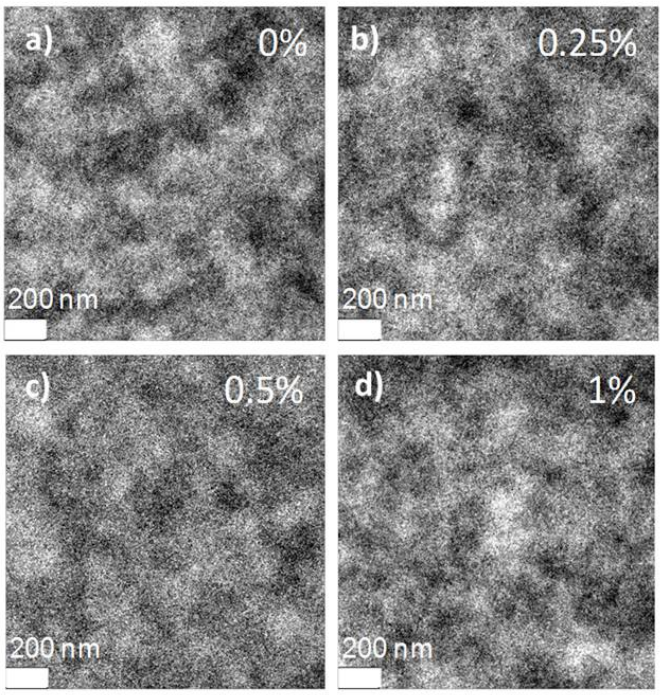

Figure 3.9: TEM images of the blends with varying doping concentration: a) undoped (0%), b) 0.25%, c) 0.5%, and d) 1% [measurements done by D. Riedel at the Ludwig-Maximilians-Universität, München]

order to analyze the pure effect of F4-TCNQ in the solar cells, a first batch with low concentration, 1:1 donor to acceptor ratio, and no solvent additives was prepared, as in the case of the charge transport measurements. Figure 3.10 shows the JV characteristics of the devices under AM 1.5G illumination. From figure 3.10, a clear increase in the J_{sc} upon doping can be seen. On the other hand, the reverse saturation current also increases reducing the FF. As reported in studies on the diode behavior of doped conjugated polymer layers, the reverse saturation dark current can be strongly increased by doping [59] as a result of the introduction of additional charge carriers. Furthermore, the devices here appear to be limited by a slight S-shape behavior, indicating poor interfaces, probably due to suboptimal morphology. However, the power conversion efficiency follows the same trend as the current and slightly increases from 1.1 % for the undoped sample to 1.3 % for the 0.3 % doped one.

Optimized devices, with donor to acceptor ratio of 1:2 in weight and diiodooctane as solvent additive, were also prepared and characterized. As can be seen

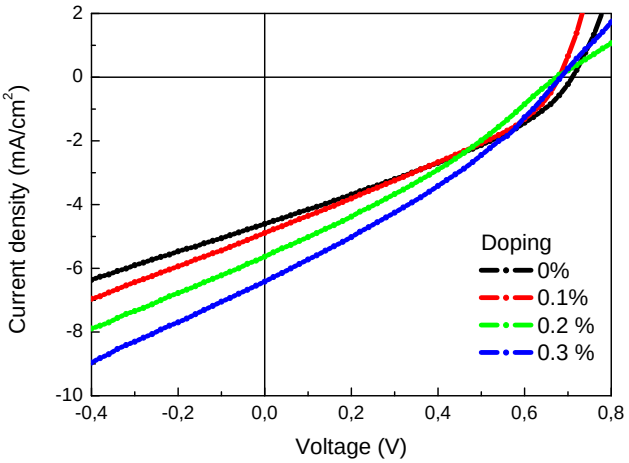

Figure 3.10: JV characteristics of the solar cells at low doping concentrations. Note that no solvent additives were used here

from figure 3.11, the performance of the reference device is improved and the power conversion efficiency increases from 1.1 % to 3.2 %. The JV characteristics of the optimized solar cells with molecularly doped active layers under AM 1.5G illumination are shown in figure 3.12. J_{sc} increases with doping up to 0.5 % as well as the efficiency, while FF stays almost unchanged. V_{oc} also slightly improves up to 0.5 %. All the parameters are found to decrease for a doping concentration higher than 0.5 %. This supports the saturation of the hole mobility for a doping

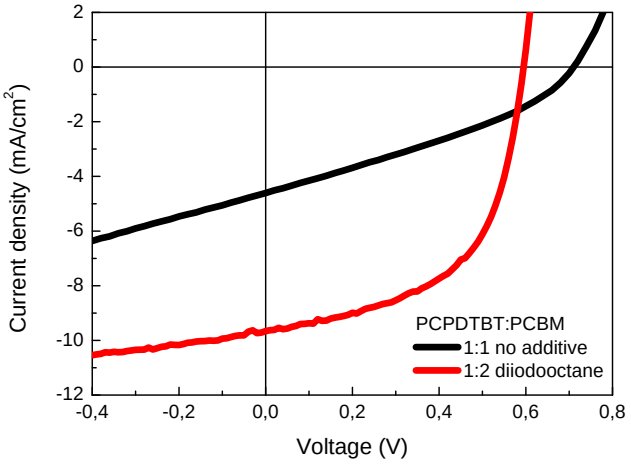

Figure 3.11: JV characteristics of the reference (undoped) PCPDTBT:PCBM solar cells before (black) and after (red) optimization of the donor to acceptor ratio and of the morphology with the use a of solvent additive

concentration around 0.3 % observed in the charge transport measurements (see figure 3.6).

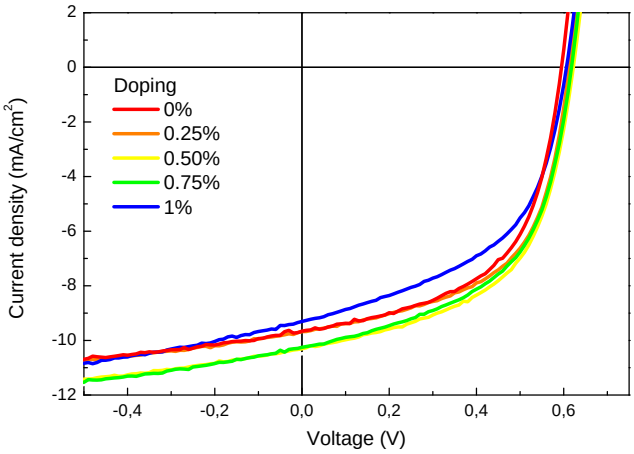

Figure 3.12: JV characteristics of the solar cells containing molecularly doped active layers. Here diiodooctane was used as solvent additive as well as an optimized donor to acceptor ratio of 1:2

Figure 3.13 summarizes the device parameters for the optimized solar cells as a function of the doping concentration. As the in-plane morphology of the blend films is not affected by molecular doping with F4-TCNQ at the investigated concentrations (figure 3.9), the changes in the photovoltaic performance of the solar cells cannot be related to the morphology of the active layer.

For what deals with the V_{oc}, it is known that it can be limited by recombination via charge transfer exciton formation [79]. By using transient photoluminescence measurements, it has been recently demonstrated that molecular doping can reduce the recombination via charge transfer excitons [72], therefore, improvements in the V_{oc} and J_{sc} of the solar cells can be regarded as a sign of reduced recombination induced by the molecular doping.

3.4 Summary

Effective molecular doping of the low bandgap copolymer PCPDTBT with F4-TCNQ is demonstrated from an increase of the sub-bandgap absorption and quenching of the PL due to the formation of ground-state complexes between the copolymer and the dopant molecule (seen from the Stern-Volmer plot). It was also found that molecular doping improves the charge transport properties by

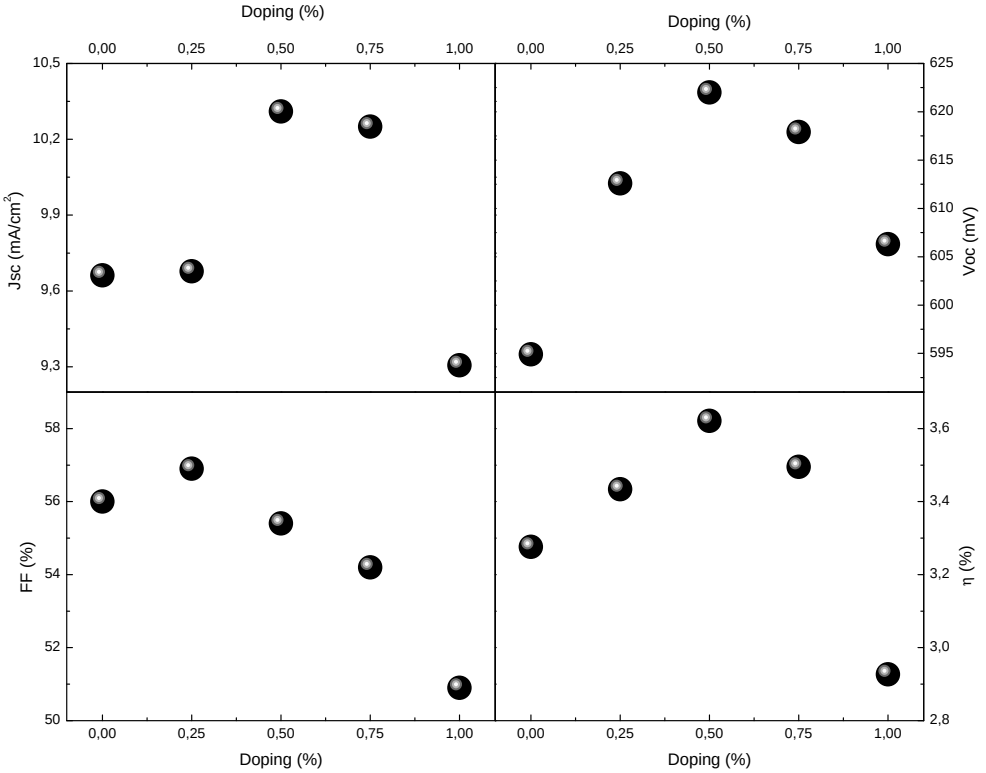

Figure 3.13: Summary of the photovoltaic performance as a function of the doping concentration for the optimized solar cells

increasing the hole mobility in both the neat copolymer and in the blend with PCBM. In these blends, molecular doping contributes to an improvement of the power conversion efficiency. In contrast, the morphology of the blend films is not influenced by the doping at concentrations below 1 %. Therefore, the observed enhancement in the hole mobility, polaron density, and photovoltaic performance is assigned to modifications of the electronic properties of the copolymer induced by the dopant.

Chapter 4

Controlling morphology with solvent mixtures

In this chapter, the effect of the solvent induced ordering on the optoelectronic, structural, and photovoltaic properties of P3HT:PCBM absorbers will be investigated using solvent mixtures. oDCB was chosen as the host solvent for all investigated blends and the relative devices as reference. CB and THN were used as co-solvents. PCBM is more soluble in both CB and THN than P3HT [44] and the use of the co-solvents is, therefore, expected to avoid PCBM clustering and allow for better arrangement of the polymer domains. More details on the sample preparation have been already presented in sections 2.1 and 2.1.1. The results presented here are adapted from A. De Sio, T. Madena, R. Huber, J. Parisi, S. Neyshtadt, F. Deschler, E. Da Como, S. Esposito, E. von Hauff, *Solvent additives for tuning the photovoltaic properties of polymer-fullerene solar cells*, Solar Energy Materials and Solar Cells 95, 3536-3542, 2011.

4.1 Effect of solvent on the optical properties of the blend

Figure 4.1 shows the normalized absorbance of the three investigated blends spun on glass. The spectra are in agreement with results found in literature for P3HT:PCBM blends, where the absorption spectrum is dominated by the $\pi - \pi^*$ absorption band of the P3HT [80], in this case peaking at about 500 nm.

The shoulder at 620 nm is an indication of the P3HT crystallinity in the layer and appears to be more pronounced in the blend deposited from oDCB:THN, indicating a higher degree of ordering [81]. In general, the absorption spectrum can slightly shift, as observed for the co-solvents cast blend, due to changes in the molecular weight of the polymer [82] or to modification of the effective conjugation length in the polymer chains, leading to slight variation of the optical bandgap [83]. The first is to be excluded, as the molecular weight does not change within the solutions. The second is dependent on the ordering of the films.

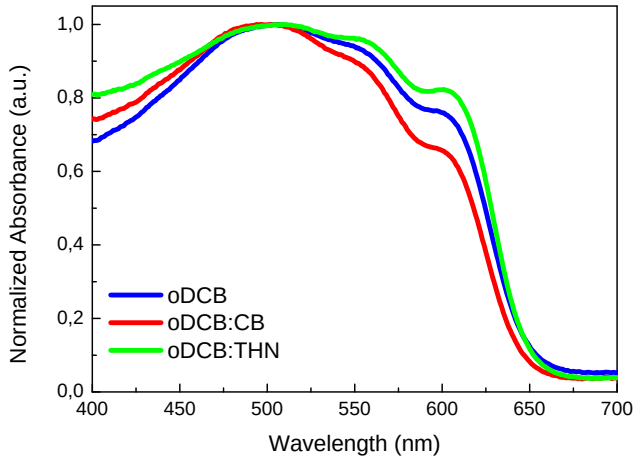

Figure 4.1: Normalized absorbance of the blends with solvent mixtures

Red shift of the spectrum and more pronounced vibronic features can, therefore, be related to morphological changes in the P3HT phase. The layers spun from the co-solvents have rather similar characteristics with different modulations in the intensity of the vibronic bands. Slight broadening of the absorption band is also visible for the oDCB:THN blend. To understand the impact of the absorption characteristics on the photocurrent of the solar cells, the expected J_{sc} for the different blends was calculated. The optical modeling of absorption and photocurrent spectra in polymer solar cells has been demonstrated in literature [84, 85] to be a powerful tool for improving light harvesting in the active layer by optimizing its thickness. Here, the optical modeling is used to understand the behavior of the J_{sc} when the absorption properties of the active layer are modified by the co-solvents.

In order to model J_{sc}, knowledge of the refractive index n and the extinction coefficient k of each layer is necessary. For ITO, PEDOT:PSS, and active layers, n and k were determined by mathematical inversion of the experimental reflectance

R and transmittance T, while for Ca and Al, used for the cathode of the solar cells, they were taken from literature [86, 87, 88]. The model of the structure used for the mathematical inversion is shown in figure 4.2.

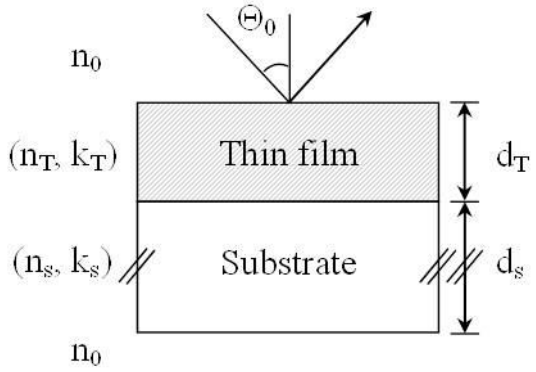

Figure 4.2: Model used to determine the optical constants

The total reflectance and the total transmittance of this structure, which are functions of the following parameters

$$\begin{aligned} R &= f_1(n_0, n_T, k_T, n_s, k_s, d_T, d_s, \theta_0) \\ T &= f_2(n_0, n_T, k_T, n_s, k_s, d_T, d_s, \theta_0) \end{aligned} \tag{4.1}$$

are expressed by the Fresnel equations. In (4.1), n_0 is the refractive index of air, n_T and k_T are the refractive index and extinction coefficient of the thin film, n_s and k_s the ones of the glass substrate, d_T and d_s the thickness of the thin film and substrate, respectively, and θ_0 is the angle of incidence of the light on the sample during the measurements. Some of the parameters in (4.1) are known or experimentally measurable. In particular, θ_0, n_0, and d_s are all known in advance, as well as d_T which can be measured. The optical constants of the glass substrate n_s and k_s are also determined by mathematical inversion. In this case, the structure to consider is air/substrate/air. Because k_s is extremely small ($k_s \ll 1$), R and T can be simplified as follows

$$\begin{aligned} R &= f_1(n_0, n_s, T_i, d_s, \theta_0) \\ T &= f_2(n_0, n_s, T_i, d_s, \theta_0) \end{aligned} \tag{4.2}$$

where $T_i = \exp(-\alpha d_s)$ is the internal transmittance of the substrate and $\alpha = 4\pi k_s/\lambda$ the absorption coefficient. For very small values of k, the internal transmittance T_i is determined with a more reasonable accuracy by mathematical

inversion than the extinction coefficient. Thus, the glass substrate was characterized by n_s and T_i. R and T of the whole structure are measured experimentally. Therefore, the equations (4.1) are solved to get n_T and k_T. A linear regression method based on the interior-reflective Newton algorithm [89, 90] is employed to extract n and k of the thin film layer.

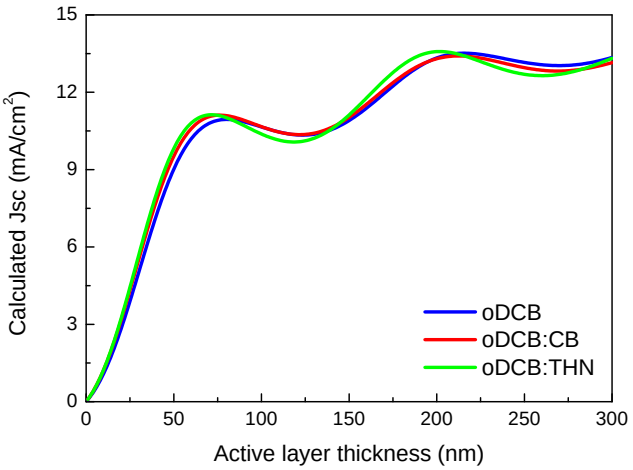

Figure 4.3: Calculated J_{sc} of the blends with solvent mixtures as a function of the active layer thickness in the ideal case of no electrical losses [simulations performed by S. Esposito at the ENEA Research Center Portici, Italy]

The optical modeling of the polymer solar cell was performed using a simulation routine based on the transfer matrix formalism [91]. The solar cell was regarded as a multilayer thin film stack in which each layer is associated with a transfer matrix based on the thickness and the complex refractive index of the layer. This method allows the computation of the reflection and transmission of the entire device and the effective absorption of the single layers in the structure. The total number of absorbed photons inside the photoactive layer was then calculated by multiplying the simulated effective absorption spectrum of this layer with the AM1.5G standard reference solar spectrum and integrating over the wavelength. The maximum current density delivered from the device is then estimated assuming that each absorbed photon results in a collected charge carrier, which means that the internal quantum efficiency (IQE) is assumed equal to one. In other words, J_{sc} obtained from the calculation is to be regarded as the maximally achievable photocurrent in the ideal case of no electrical losses in the device. The results of the J_{sc} modeling are shown in figure 4.3.

For the thickness values investigated here (115 nm for oDCB, and 130 nm

for oDCB:CB and oDCB:THN), only a minimal difference in J_{sc} is expected, with oDCB:THN showing the lowest current. The oDCB:CB system is optically similar to the oDCB reference system. The oDCB:THN system, on the other hand, has the potential to deliver a higher photocurrent if thicker layers are employed. Thicker absorber layers, however, can lead to recombination losses due to the low diffusion lengths of the charge carriers.

4.2 Effect of solvent on the structural properties of the blend

The variation of the in-plane morphology induced by solvent mixing was investigated with transmission electron microscopy (TEM). The TEM images of the three blends are shown in figure 4.4. The lighter regions are attributed to the polymer rich phase, while the darker regions to fullerene rich domains [92]. An enhanced phase segregation between polymer and fullerene domains in the mixed solvent blends is evident, in comparison to the blend cast using the host solvent alone. The domain sizes of both polymer and fullerene appear larger, and lamellae-like structures can be seen in the P3HT. In the blend cast from oDCB, the PCBM domains are still recognizable, however the phase segregation between polymer and fullerene domains is not as clear. It is also possible that molecularly dispersed PCBM in the polymer domains disturbs the phase segregation and creates recombination centers [93]. In presence of well defined polymer and fullerene pathways for the transport of charge carriers, a higher photocurrent in the solar cells is expected.

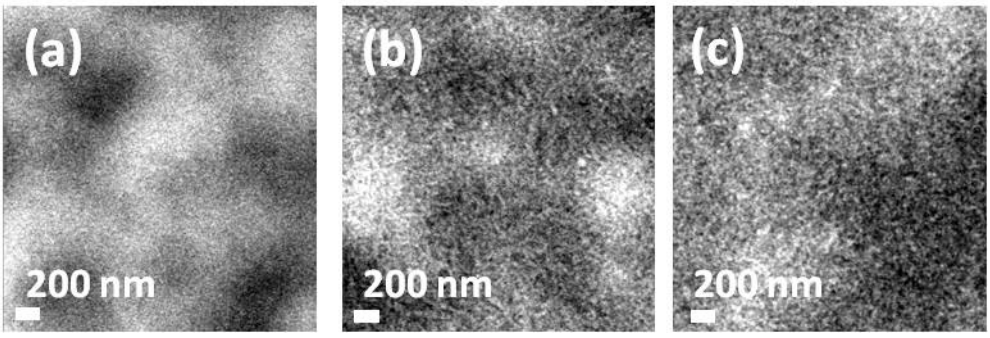

Figure 4.4: TEM image of the blend films deposited from (a) oDCB, (b) oDCB:CB, and (c) oDCB:THN [images taken by S. Neyshtadt at the Ludwig-Maximilians-Universität, München]

To get better insights into the morphology of the active layer for the three different blends, AFM and KPFM were exploited. Combining these techniques, it was possible to analyze the surface composition, surface roughness, and surface potential of the blends. It was found that the blend prepared from oDCB and oDCB:CB have comparable RMS surface roughness, while the one cast from oDCB:THN shows RMS roughness more than four times higher. It has been reported that there is a positive correlation between the surface roughness of the blend and the efficiency in bulk heterojunction solar cells [94, 95].

Blend	**RMS Surface roughness** (nm)	**Surface potential** (eV)
oDCB	1.08	-5.272
oDCB:CB	0.92	-5.160
oDCB:THN	4.62	-5.068

Table 4.1: Surface roughness and surface potential of the blends [measurements by T. Madena at the Universität Oldenburg]

KPFM can be employed to determine the polymer and fullerene content at the surface of the blend [96]. In table 4.1, the positions of the peak of the surface potential taken from the KPFM scans of the blends are reported. The surface potential values of the blends (histograms are not shown here) have values between roughly -4.9 and -5.5 eV, with well defined and unique peaks for each blend [97]. The shift in the surface potential between the reference blend and the blends cast from the co-solvents is attributed to increased crystallinity in the P3HT phase, known to influence the HOMO level of the polymer [98]. The blend cast from oDCB:THN demonstrates the highest P3HT crystallinity at the surface, and the blend cast from oDCB the lowest.

These results indicate that a suitable choice of the co-solvent can have a positive impact on film formation and morphology. For the scan resolution of the KPFM measurements (20 nm), there was no evidence of PCBM on the surfaces of the blends. This is consistent with previous findings from literature that reported accumulation of the polymer at the top of the blend layer and the fullerene at the bottom [32, 99, 100].

4.3 Effect of solvent on the electrical properties of the blend

CELIV was employed to examine the transport properties of the charge carriers in the three different blends. In contrast to other techniques, such as field-effect mobility or time of flight measurements, CELIV allows to study the steady state transport properties directly in the solar cell geometry. This is advantageous when studying variations in the transport properties due to changes in the active layer morphology. The dark transport characteristics were investigated here to determine the role of transport on the photocurrent in the different blends. For ambipolar blends, this technique has been applied to analyze the mobility and recombination effects in organic solar cells [101]. For the blends investigated here, the values of the zero-field mobility are reported in table 4.2.

Blend	**Zero-field mobility** $(cm^2V^{-1}s^{-1})$
oDCB	5.7×10^{-5}
oDCB:CB	4.2×10^{-5}
oDCB:THN	2.3×10^{-6}

Table 4.2: Dark mobility measured with CELIV [measurements by R. Huber at the Universität Oldenburg]

CELIV does not allow to distinguish between electron and hole transport, but the faster carriers are detected. It has been reported that in P3HT:PCBM blends, measured with a number of different techniques, the electron mobilities are consistently higher than the hole mobilities [102, 103]. For this reason, the mobility values in table 4.2 refer to electrons in the blend. Blends cast from oDCB demonstrate the highest electron mobility while blends cast from oDCB:THN the lowest one. The accumulation of P3HT at the top of the blend, previously assessed with KPFM 4.2, is expected to inhibit electron transport to the cathode of the device, resulting in a decrease in the bulk electron mobility.

4.4 Effect of solvent on the photovoltaic performance

Polymer:fullerene bulk-heterojunction solar cells were fabricated according to the recipe reported in section 2.1.1. The photovoltaic performance of the investigated blends are summarized in table 4.3, and the JV characteristics are

Blend	$\mathbf{J}_{sc}$ (mA/cm^2)	$\mathbf{V}_{oc}$ (mV)	**FF** (%)	η (%)
oDCB	5.53	580	58.63	1.88
oDCB:CB	6.65	600	48.12	1.91
oDCB:THN	7.42	590	49.36	2.16

Table 4.3: Photovoltaic performance of the investigated blends

plotted in figure 4.5. While the values of V_{oc} are comparable among the cells, the values of the photocurrent of the devices prepared using the co-solvents are both higher than that of the reference cells prepared from the host solvent, with the oDCB:THN blend resulting in the highest J_{sc}.

The significant differences in J_{sc} between the cells investigated are attributed to improvements in the ordering of the polymer phase in the mixed solvent blends compared to the reference system. Increased crystallinity in the P3HT phase is known to lead to slight decreases in V_{oc} due to upward shifts in the HOMO level of the polymer [98]. V_{oc} can be further limited by recombination at the contacts. Interestingly, FF is negatively influenced by the co-solvents. However, because of the relatively large increase in J_{sc} compared to the decrease in FF, the power conversion efficiency (η) of the devices improves when using the co-solvents, from 1.88% for oDCB to 2.16% for oDCB:THN.

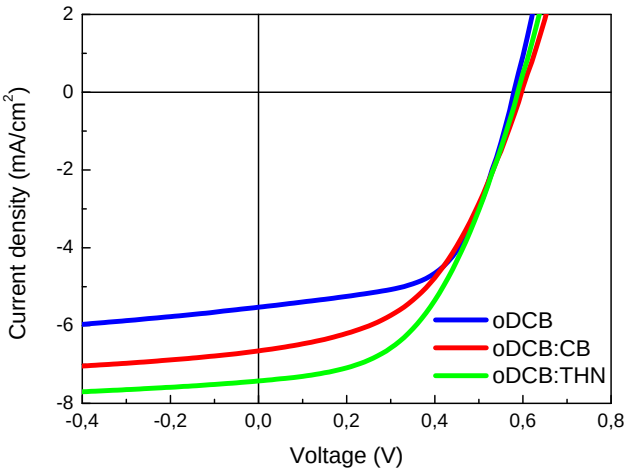

Figure 4.5: JV characteristics of the solar cells with solvent mixtures

In figure 4.6, the external quantum efficiency (EQE) spectra of the investigated solar cells are shown. In agreement with the JV characteristics (figure 4.5), the oDCB:THN blend demonstrates the highest photocurrent, while the blend

prepared from pure oDCB the lowest one. It is interesting to note that the EQE spectrum of the reference oDCB solar cell presents a drop between 350 and 450 nm that is not apparent in the devices prepared from co-solvents. The total signal is also much lower. This behavior has been observed in P3HT:PCBM cells having poor ordering of the polymer domains [92]. The EQE spectra suggest that the co-solvents induce a more favorable ordering in the blend, leading to improvements in the photon to electron conversion efficiency and, therefore, in the photocurrent.

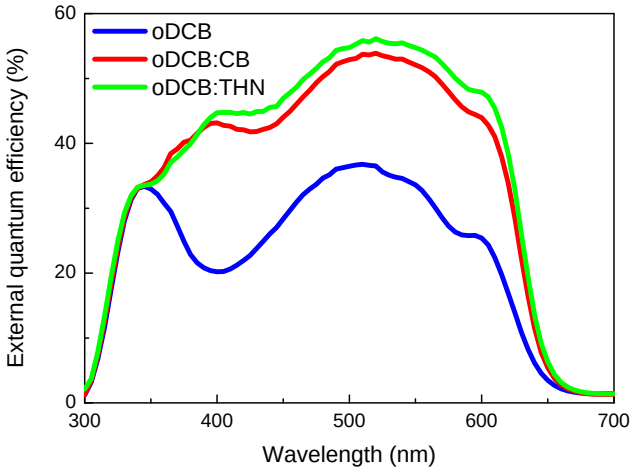

Figure 4.6: EQE spectra of the solar cells with solvent mixtures

4.5 Summary

The results presented demonstrate that the morphology of polymer:fullerene solar cells can be tuned using co-solvents with different boiling point with respect to the host solvent. The increase in J_{sc} of the solar cells corresponds to enhanced phase segregation between the polymer and fullerene phases in blends prepared with solvent mixtures (as measured from TEM) and increased polymer ordering (seen from KPFM). On the other hand, it was observed that the higher P3HT crystallinity negatively impacts the electron transport in the blend, as illustrated by the decrease in FF of the solar cells and by the bulk electron mobility measured using CELIV. Despite this, an increase in the overall photocurrent and device efficiency is observed when using solvent mixtures. The photocurrent is determined primarily by light absorption leading to photogenerated excitons, and

subsequently by the separation and transport of charge. Therefore, the results reflect improvements in charge separation between the donor and the acceptor due to improved morphology. While improvements to the in-plane morphology are important for charge separation, an optimal vertical segregation [104] of the blend is required for efficient charge collection. Structural investigations with TEM, KPFM, and AFM indicate that the solvent mixtures lead to preferential in-plane phase segregation between the polymer and fullerene and to increased P3HT ordering in the blends. The trend in the electron mobility between the blends is consistent with the KPFM data and the drop in the FF resulting from the increased crystallinity in blends cast from mixed solvents. It is interesting that while the electron mobility decreases with increasing P3HT ordering, the overall photocurrent in the solar cells is improved.

Chapter 5

Optimization of the device architecture

In most organic optoelectronic devices, including solar cells and light-emitting diodes, the front electrode is based on a transparent conducting oxide (TCO) that, in most cases, is indium tin oxide (ITO). Although it shows high transmission and conductivity, ITO is one of the main cost consuming elements in present photovoltaic devices, due to the scarce reserves of indium in nature, and is also potentially harmful [105]. Polymer:fullerene solar cells in the standard forward architecture typically use ITO as the anode, covered with a solution processed buffer layer that serves as hole transporting layer, usually PEDOT:PSS, and a low work function metal as the cathode. PEDOT:PSS, normally available as a water dispersion, is highly hygroscopic which makes the ITO/PEDOT:PSS interface extremely sensitive to ambient air. Furthermore, the acidic character of the PSS component facilitates the chemical degradation of the ITO [106].

It is also questionable whether the standard forward structure of the bulk heterojunction solar cells is optimal. It was demonstrated in several studies that a spontaneous vertical phase separation occurs in spin coated polymer:fullerene blends, leading to a concentration gradient in the active layer with fullerene-rich regions near the substrate side and polymer-rich ones adjacent to the free surface [99, 32] which can reduce both the performance and the reproducibility of the device [107].

Furthermore, the facile oxidation of the low work function metals used for

the cathode represents an inherent instability that demands for encapsulation of the devices, in order to prevent degradation due to air exposure. Reversing the device polarity by fabricating an inverted structure removes the danger of exposing the low work function electrode directly to air [108, 109] and, at the same time, can even turn the spontaneous arrangement of the materials in the active layer into a positive feature. However, the complete removal of air instable electrodes would be more desirable to make the device more robust. An inverted device architecture, in which the negative electrode is at the bottom of the stack and in which ITO is replaced with a less expensive TCO, should, therefore, be beneficial for solar cell stability, cost and performance.

It has been reported that *aluminum doped zinc oxide* (ZnO:Al) can be employed as alternative to ITO in standard small molecule [110] and polymer solar cell structures [111]. However, its use in inverted polymer solar cells has been limited likely due to poor performance.

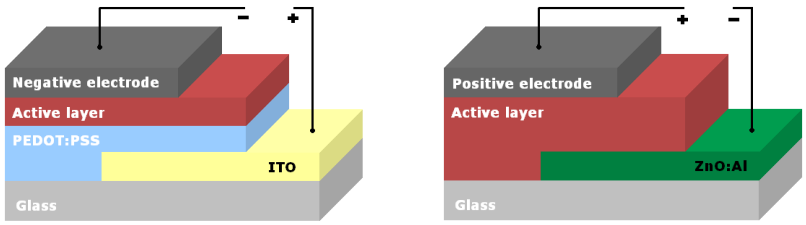

Figure 5.1: Device structure of the standard forward architecture on ITO (left) and the inverted ITO-free one (right)

In this chapter, an inverted architecture based on ZnO:Al is presented. The use of low work function metals and materials that could accelerate the degradation of the devices will also be avoided. The layer sequence for the commonly used forward structure on ITO (left) and the ITO-free inverted cell architecture (right) proposed in this chapter are depicted in figure 5.1. The results presented here are adapted from A. De Sio, K. Chakanga, O. Sergeev, K. von Maydell, J. Parisi, E. von Hauff, *ITO-free inverted polymer solar cells with ZnO:Al cathodes and stable top anodes*, Solar Energy Materials and Solar Cells 98, 52-56, 2012.

5.1 ZnO:Al as TCO for polymer:fullerene solar cells

Neat ZnO layers are highly transparent in the visible range, but present low electrical conductivity. The latter can be boosted by doping with group III

elements, such as Ba, Al, Ga, and In [112]. From reports on the effect of impurities in ZnO emerges that the best dopants to obtain transparent and conducting films are Al and Ga, with Al resulting in the lowest electrical resistivity [113]. ZnO:Al films show good transmittance in the visible and near-infrared regions and have been already employed as TCOs in various types of inorganic solar cells [114, 115, 116]. The Al content has a high impact on the structural, electrical and optical properties of the ZnO:Al films. By varying the doping concentration, changes in the grain size, electrical resistivity and refractive index of the material were observed [117]. The direct bandgap of the ZnO:Al also varies with doping [117]. Al acts as n-type substitutional dopant in the ZnO matrix, replacing the Zn atoms in the crystal structure. The introduction of Al atoms in the ZnO increases the density of electrons and, therefore, the conductivity. At the same time, the transmittance in the near-infrared range is reduced. For high doping levels, excess Al forms nonconductive Al_2O_3 clusters, leading to a drop in the conductivity [118]. Here, the Al concentration in the films was found to be of 0.94% weight by weight (w/w), from energy dispersive X-ray spectroscopy (EDX) measurements. In addition to the composition, the substrate temperature during the deposition has a strong impact on the ZnO:Al properties [119]. This parameter, however, is beyond the scope of this study, therefore, the temperature was fixed at 400°C for all the samples. More details on the preparation of the ZnO:Al are reported in section 2.3.

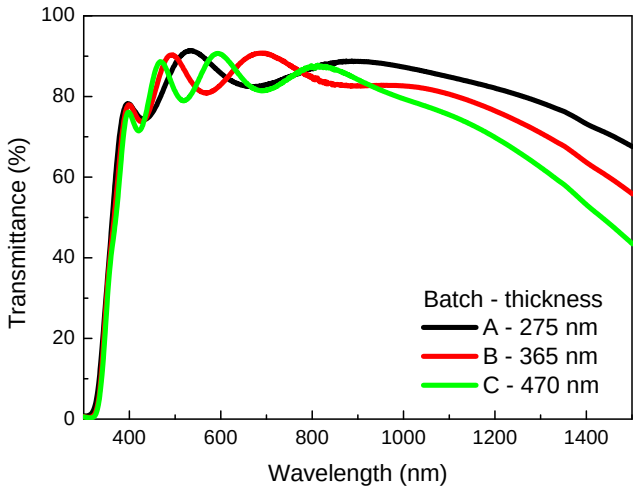

Figure 5.2: Transmittance of ZnO:Al layers with different thickness [measurements by K. Chakanga at the EWE Research Center Next Energy, Oldenburg]

The basic requirements for a TCO to be suitable for electronic applications are high transmittance over a broad spectral range and low sheet resistance. These two parameters follow opposite trends. Therefore, a trade-off has to be accepted. In order to obtain a good compromise between sheet resistance and transmittance, three ZnO:Al batches (A, B, C) with varying thickness were fabricated and characterized. The transmittance of a representative sample for each batch is shown in figure 5.2 together with the respective thickness.

With increasing layer thickness, the sheet resistance of the layers decreases from 20 to 13 Ω/□ and, at the same time, the average transmittance decreases and more interference fringes appear in the visible range of the spectrum. The average surface roughness also increases with the thickness, from 1.5 nm for batch A to 4.5 nm for batch C. The batch with the highest transmittance and the lower number of fringes, i.e., the one with the thinnest and smoothest layers, was chosen as the best compromise. To summarize, the ZnO:Al layers used to fabricate the polymer:fullerene solar cells are 275 nm thick, have an average sheet resistance of 20 Ω/□ and a surface roughness RMS of 1.5 nm. The commercial ITO thin films used in this study are instead 180 nm thick, have an average sheet resistance of 8 Ω/□ and an RMS roughness of 3.9 nm. Thus, in comparison to the commercial ITO, the sheet resistance of the ZnO:Al is higher, but its surface is smoother.

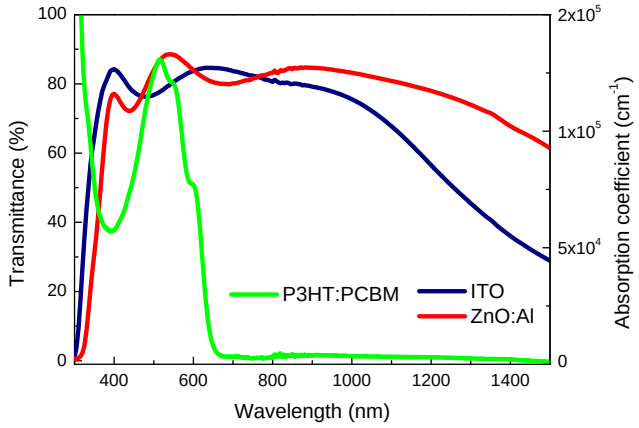

Figure 5.3: Transmittance of the ITO and ZnO:Al layers compared to the absorption coefficient of the P3HT:PCBM

In figure 5.3, the transmittance of ITO and ZnO:Al together with the absorption coefficient of the active layer are depicted. The average transmittance in the range where the polymer:fullerene blend absorbs is 78% for ITO and 85% for ZnO:Al. Therefore, the transmittance of the ZnO:Al matches better the absorp-

tion of the blend used for the active layer (figure 5.3) with respect to ITO. In this case, a higher amount of incident light is able to reach the active layer, when using the ZnO:Al as TCO. The transmittance of the ZnO:Al is markedly higher than ITO also in the near-infrared range. Therefore, low bandgap polymers [66] could also benefit from the improved optical matching of the ZnO:Al compared to ITO.

5.2 ITO-free polymer:fullerene solar cells

The inverted solar cells with ZnO:Al as the TCO were preprared without using low work function metals for the electrodes and without water based buffer layers. For the active layer, P3HT:PCBM was chosen. More details on the device preparation can be found in section 2.1.1. The structure of the inverted cells is shown in figure 5.1 on the right hand side. The high quality and surface smoothness of the ZnO:Al thin films allow to process the active layer directly on the top of the TCO without the need to employ additional interlayers or surface treatments to enhance the adhesion of the organics. This is remarkable from the point of view of the device manufacturing.

In order to optimize the device performance, the impact of the anode in the inverted structure was also investigated. At first, a simple structure, in which the P3HT:PCBM active layer is sandwiched directly between the ZnO:Al cathode and an Au anode, was fabricated. For this inverted architecture, a power conversion efficiency of only 0.63% has been obtained. From figure 5.4 (black line), it can be seen that both V_{oc} and FF are too low for the P3HT:PCBM blend used for the active layer. This indicates poor charge collection at the electrodes. The unsatisfactory results can be mainly attributed to a bad interface between the organic active layer and the Au anode. Therefore, Au was replaced with a thin layer of MoO_3, a transition metal oxide with a suitable bulk work function [120], covered with 100 nm of Ag. Several reports from literature have investigated the influence of MoO_3 on the solar cell performance [121] and stability [122, 123].

As can be seen from figure 5.4 (green line), the solar cells show increased V_{oc} and FF with only 2 nm of MoO_3. In particular, V_{oc} increases from 290 to 506 mV and the FF from 35 to 47% when MoO_3 is used between the active layer and the metal anode. J_{sc} is also significantly improved, and the devices achieve a power conversion efficiency of 2.47%. The enhancement can be attributed to

a better work function alignment, but also to beneficial doping of the organic layer when using MoO_3. It is well known that the work function of a thin film differs from the one of the same material in the bulk. In the case of thin Au layers, for example, a variety of different values ranging from 4.2 to 5.4 eV are reported in literature [124, 125]. It has been recently observed that thermally evaporated thin Au films exposed to ambient air have a work function significantly lower than the one measured for the same Au surface that was not exposed to air [126]. Additionally, the interfaces formed by thermal evaporation of metals on organics are not abrupt, but consist of ultrathin layers of organo-metallic compounds formed due to the diffusion of hot metallic atoms into the organic layer [127] during the evaporation, leading to doping of the active layer. Furthermore, thermally evaporated transition metal oxides, such as MoO_3 and V_2O_5, were observed to form islands during the growth [121]. Consequently, a 2 nm thin layer is probably not uniform and leads to only a partial coverage of the active layer, which is, therefore, also in contact with the Ag layer. This impacts V_{oc} of the solar cells, meaning that the performance of the inverted devices could be further improved, if the optimal thickness for the anode interlayer is used. In fact, the thickness of the MoO_3 layer has been observed to influence the device parameters. In similar inverted structures fabricated on fluorine-doped SnO_2 substrates, an optimal thickness of 15 nm was reported [128], while for a standard forward solar cell structure on ITO, 5 nm was found to be the optimal thickness

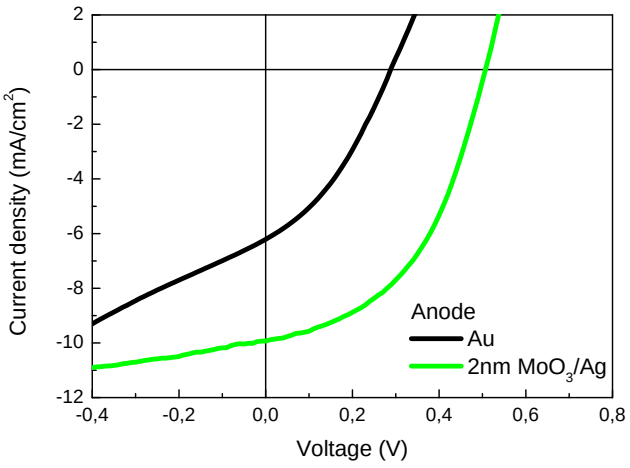

Figure 5.4: JV characteristics of the inverted ZnO:Al devices with Au (black line) and MoO_3/Ag (green line) top contacts under AM 1.5G illumination

[129]. This indicates that the thickness of the MoO_3 layer should be optimized when changing the device architecture. For these reasons, the effect of a thickness variation of the MoO_3 interlayer was investigated.

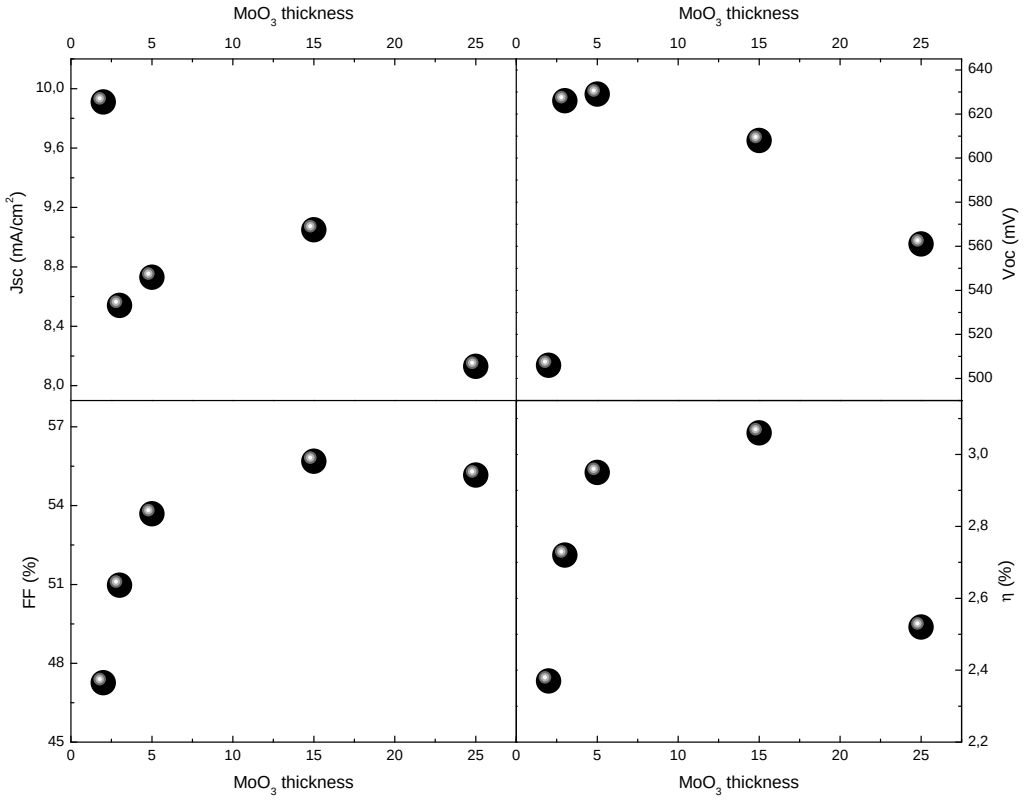

Figure 5.5: Effect of the thickness of the MoO_3 anode interlayer on J_{sc}, V_{oc}, FF and η of the inverted ZnO:Al solar cells

Inverted solar cells on ZnO:Al substrates with an anode interlayer thickness ranging from 2 to 25 nm were prepared and characterized. Figure 5.5 summarizes the solar cell parameters with different MoO_3 interlayer thickness. An evident trend with a maximum at 15 nm thick MoO_3 is shown for FF and the power conversion efficiency. J_{sc} shows a kind of slight oscillation, probably as a result of interference effects upon thickness variation. It is possible that the MoO_3 interlayer also acts as an optical spacer, redistributing the optical field in the solar cell. This behavior is thickness dependent and has already been demonstrated for TiO_x [130] and ZnO [85] optical spacers in forward device architectures based on ITO. For an interlayer thickness above 5 nm, V_{oc} slightly decreases. This can result from increased potential drop across the thicker MoO_3 interlayer. The low initial value of 506 mV for a 2 nm thick MoO_3 is attributed to a poor contact

between the electrode and the active layer. However, the optimal MoO_3 thickness for the geometry investigated here (figure 5.1), is 15 nm.

The substitution of the PEDOT:PSS anode buffer layer with the more stable MoO_3 is expected to improve the device lifetime. It has already been reported that solar cells based on small molecules in which the ITO is covered by a thin layer of MoO_3 instead of PEDOT:PSS are more stable under illumination [131]. It was also recently shown that ITO-based inverted cells without PEDOT:PSS achieve a shelf lifetime of 15 days, while the standard forward cells containing PEDOT:PSS only half a day [132]. The absence of both water based buffer layers and low work function metals in the ITO-free inverted structure should further improve the air stability of the devices.

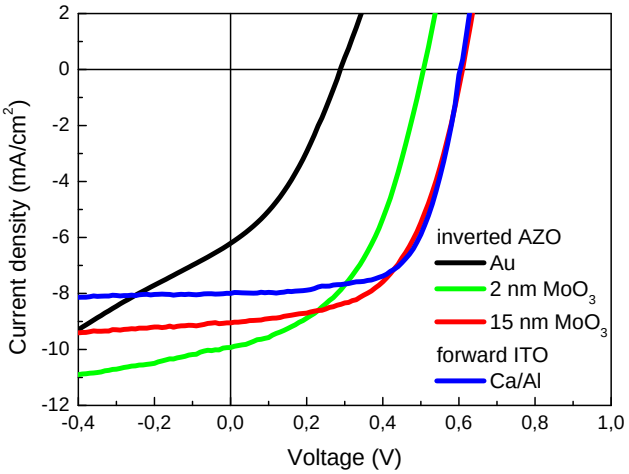

Figure 5.6: JV characteristics of the inverted ZnO:Al and forward ITO cells under AM 1.5G illumination. For the inverted devices, the performance of the different anodes are shown: Au, 2 nm MoO_3, and 15 nm MoO_3 interlayer

The optimized inverted cells led to a device efficiency comparable to those of the reference ITO-based devices. Figure 5.6 shows the JV curves of the inverted and forward solar cells investigated. For the optimized inverted ZnO:Al based device with 15 nm MoO_3 anode buffer layer (figure 5.6 red line), J_{sc} is 9.05 mA/cm^2, V_{oc} 608 mV, FF 56.00% and η 3.08%, while for the standard ITO-based device (figure 5.6 blue line), J_{sc} is 7.99 mA/cm^2, V_{oc} 604 mV, FF 64.35%, and η 3.10%. The higher J_{sc} of the ZnO:Al based cell, due to better light coupling, can be clearly seen from the data. V_{oc} of the two device architectures are similar. This is an indication that the work functions of the anode and cathode result in comparable charge carrier extraction efficiency in both the inverted and the

standard forward devices. The lower FF of the inverted cells, however, could be attributed to surface recombination at the ZnO:Al/active layer interface. In fact, while in the forward structure buffer layers are used at both the ITO anode (PEDOT:PSS) and the Al cathode (Ca), in the inverted structure, there is a MoO_3 buffer layer at the anode, but no buffer layer at the cathode, where the ZnO:Al is in direct contact with the active layer. In this case, surface defects due to the deposition process and recombination at the interface can adversely affect FF. Regarding the TCO features, it is interesting to note that the higher sheet resistance of the ZnO:Al, compared to the one of the ITO, is not a limiting factor for the solar cell performance. This is an important result when considering the optimization of TCOs for use in organic solar cells.

5.3 Summary

Efficient ITO-free inverted solar cells with ZnO:Al cathodes and MoO_3/Ag anodes were produced and optimized. Efficiencies comparable to ITO based devices prepared in the standard forward structure were achieved. This demonstrates that ZnO:Al is a convenient and valid alternative to ITO. The thickness of the ZnO:Al was optimized so that a good compromise between sheet resistance and transmittance was obtained. The MoO_3 buffer layer was also optimized to further improve the efficiency of the photvoltaic devices. The inverted polymer:fullerene solar cells show a higher photocurrent than the standard ITO devices due to the higher transmittance of ZnO:Al in the spectral region where the P3HT:PCBM blend absorbs. The higher sheet resistance of the ZnO:Al compared to the one of ITO does not adversely affect the device performance. From the point of view of the device stability and manufacturing, the inverted architecture is more attractive, because water-based transport layers and low work function metals are avoided without sacrificing the device efficiency.

Chapter 6

Effect of degradation on the optoelectronic properties of P3HT and P3HT:PCBM blends

The literature about the stability of polymer solar cells mainly focuses on the complete devices [50, 133, 134, 135, 136]. Although the effect of degradation on the whole photovoltaic device is important, it is sometimes not possible to determine the effect on the single layers. For example, it is not always possible to distinguish the role of the active layer from that of the electrodes [137]. It has been shown that the device structure plays also a role and that some structures are more prone to degradation than others. Whereas in forward devices the degradation of the low work function metal used as the top electrode limits the lifetime [135], it has been recently shown that in inverted structures the electrodes do not play the same crucial role [138]. An important issue is the understanding of the degradation mechanisms in the active layer. Therefore, in this chapter, the degradation of P3HT layers and its blend with PCBM will be investigated. Although there are new promising conjugated polymers, P3HT has still high relevance in the field of polymer photovoltaics. In fact, P3HT is one of the most investigated polymers in literature and is often regarded as a model system. From the point of view of the device lifetime, deep understanding of the degradation

mechanisms in P3HT will open the way for the design and synthesis of new polymers with enhanced stability.

Part of the results presented in the second part of this chapter are adapted from F. Deschler, A. De Sio, E. von Hauff, P. Kutka, T. Sauermann, H.-J. Egelhaaf, J. Hauch, E. Da Como, *Effect of ageing on exciton dynamics, charge separation and recombination in P3HT/PCBM photovoltaic blends*, Advanced Functional Materials, 2012, accepted.

6.1 The influence of the processing atmosphere

It is assessed that most polymers experience more or less rapid degradation when exposed to air and light [50]. For this reason, when investigating new material combinations and new device architectures, the experiments are mainly performed on samples prepared in an inert atmosphere, such as nitrogen filled gloveboxes. This is of course not convenient for industrial production of photovoltaic devices based on conjugated polymers. In fact, while the preparation of the solutions or inks in an inert atmosphere is feasible, processing the whole devices in a glovebox is clearly time and cost consuming when dealing with large scale manufacture. On the other hand, in order to understand the fundamental mechanisms that rule the photovoltaic action of conjugated polymers, the effect of degradation has to be first neglected. Therefore, most studies report investigations and findings based on samples prepared, and sometimes even measured, in the glovebox. Once the polymer behavior under inert conditions has been assessed and the devices have been optimized, the next step towards the design of more robust materials, as well as device architectures, should be the understanding of the material and device behavior when exposed to ambient air. Therefore, in this section, the effect of the processing environment on the optoelectronic properties of the reference polymer P3HT and on the relative devices is investigated. For this purpose, pristine rr-P3HT layers and blends with PCBM were prepared under nitrogen atmosphere and in ambient air, using solutions prepared in the glovebox. More details on the samples preparation can be found in 2.4.

6.1.1 Optical and photophysical properties

Figure 6.1 shows the absorption coefficient of two P3HT samples prepared inside and outside the glovebox as a function of the wavelength. It can be seen

that the overall absorption coefficient is lower when processing in air. Moreover, the typical absorption features of the P3HT become less pronounced, with the absorption maximum even blue shifting from 515 nm for the sample prepared under nitrogen to 498 nm for the one cast in air. The shoulder around 600 nm also slightly blue shifts and becomes less pronounced, indicating that in the film spun in ambient air a lower degree of ordering is achieved. The absorption edge, however, does not significantly change.

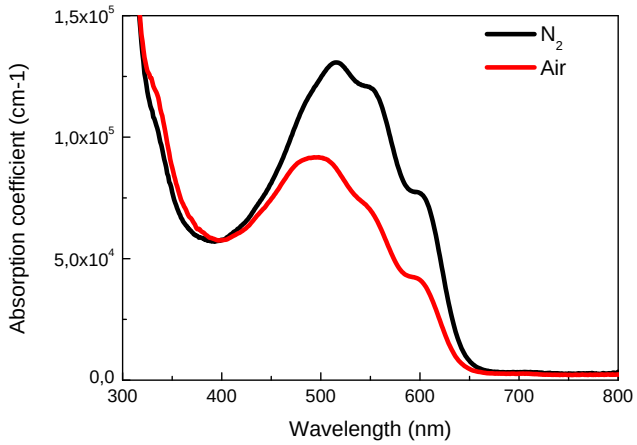

Figure 6.1: Absorption coefficient of P3HT layers processed in nitrogen (black) and in ambient air (red) as a function of the wavelength

Figure 6.2 reports the PL spectra of the samples prepared in nitrogen (black line) and in air (red line). The spectra were corrected for the optical density of the respective samples at the laser wavelength (532 nm), in order to get rid of the difference in absorption and thickness. The shape of the PL signal is similar in both samples.

It can be seen that processing in air leads again to a decrease in the signal intensity, compared to samples prepared under nitrogen. The ratio of the area of the PL in air and in nitrogen is 0.82. The lowering of the PL intensity can be regarded as resulting from the interaction of the oxygen with the P3HT. In fact, oxygen is known to be a luminescence quencher for many organic molecules [139]. However, here the samples were exposed not to pure oxygen, but to ambient air. Therefore, the effect of the interaction with air humidity is also to take into account. Although it is not clear what the effect of humidity on the polymer is, complete photovoltaic devices were observed to degrade faster when containing PEDOT:PSS [132]. Investigations on PPV based solar cells assigned such rapid

degradation to reabsorption of water from the hygroscopic PEDOT:PSS buffer layer [140]. Other experiments to probe the effect of humidity on the performance of polymer solar cells [141] reported diffusion of water through the complete devices. However, it is not possible to completely exclude that humidity has a detrimental effect on the P3HT itself, because it is not trivial to distinguish and isolate the role of humidity from the one of oxygen alone on the active layer.

To probe the effect of the processing environment on the excited species, steady-state PIA was measured on the same layers. The PIA spectra of the samples processed in different atmospheres are shown in figure 6.3. In order to compare the spectra, normalization for the ground state bleaching was performed. The spectrum of the pristine P3HT (black line) is in good agreement with results from literature [142, 143], where the features at 1.07 eV and 1.25 eV are assigned to singlet excitons and to localized intrachain polarons [142, 144], respectively. The small peak at about 1.15 eV, visible in the sample cast in the glovebox, is an artifact resulting from the measurement.

From figure 6.3, it can be seen that processing in air leads to a variation in the PIA signal. A small decrease in the characteristic P3HT features is observed. In particular, the singlet exciton population decreases, while the localized polaron peak experiences a slight red shift without changing its intensity. More obviously, a new broad band from 1.4 to 1.9 eV emerges. This band consists of a peak at 1.68 eV and a shoulder at 1,81 eV. Based on steady-state measurements only, it is not

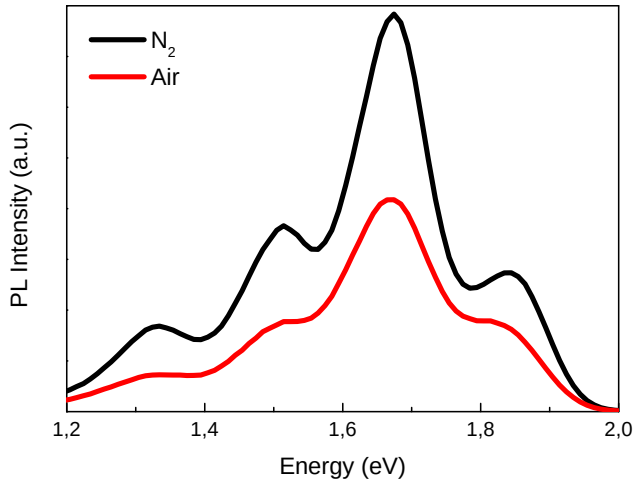

Figure 6.2: PL spectra of P3HT layers processed in nitrogen (black) and in ambient air (red)

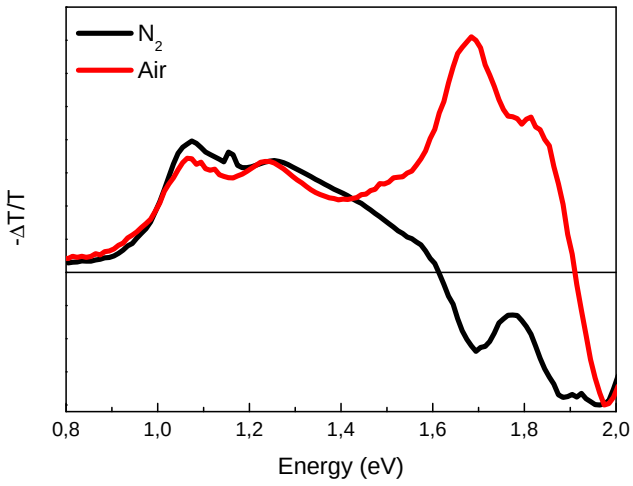

Figure 6.3: PIA spectra of the P3HT layers processed in nitrogen (black) and in ambient air (red)

possible to assign the nature of this new excited species. However, a photoinduced absorption band between 1.6 and 1.9 eV is observed, when blending conjugated polymers with the fullerene C_{60} [145] or its derivative PCBM, and is assigned to delocalized interchain polarons. From figure 6.3, a blue shift of the zero crossing is also visible, meaning that the emission from the sample is inhibited due to the interaction with ambient air during film formation.

6.1.2 Photovoltaic performance

To understand the impact of the change in the optoelectronic properties of the P3HT due to degradation in the photovoltaic devices, bulk-heterojunction solar cells based on P3HT:PCBM blends were prepared. The active layer was spun in and outside the glovebox, while the other processing steps were common to both kinds of samples. A detailed recipe can be found in chapter 2. To evaluate the differences in the samples based only on the absorption properties, the photocurrent was simulated. An optical modeling was performed according to the procedure already explained in section 4.1. Figure 6.4 shows the calculated J_{sc} for the solar cells with the active layers processed in nitrogen (black line) and in air (red line). As already pointed out in section 4.1, the calculation does not take into account any electrical loss in the device.

From figure 6.4, it can be seen that the calculated J_{sc} is lower when processing the samples in ambient air for an active layer thickness below 300 nm. The

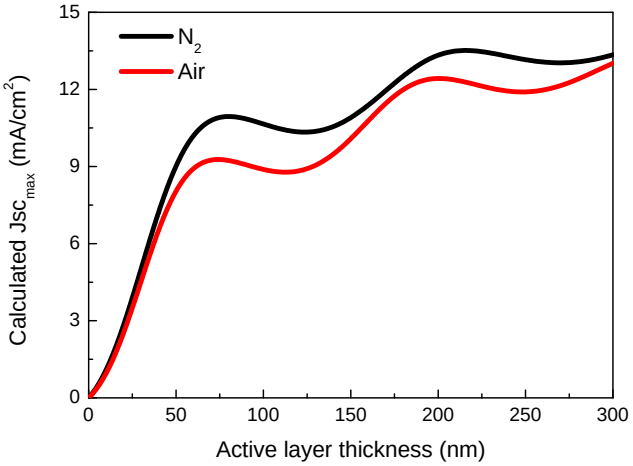

Figure 6.4: Calculated J_{sc} of the P3HT:PCBM solar cells processed in nitrogen (black) and in ambient air (red) as a function of the active layer thickness [simulations by S. Esposito at the ENEA Research Center Portici, Italy]

position of the maxima and minima shift to a lower thickness, when preparing the sample in air. In fact, the maxima occur at 80 nm and 216 nm for the sample prepared in nitrogen, while for the one cast in air the positions are 74 nm and 201 nm, respectively. The first minimum shifts also from 124 nm to 113 nm, when processing in air. This means that the maximum calculated photocurrent is achieved with slightly thinner active layers for devices prepared in ambient air. On the other hand, the value achieved is lower with respect to devices processed under inert atmosphere. For the solution concentration used in this experiment, the active layer was about 130 nm thick for both devices. From the optical modeling, the ratio of J_{sc} in air and in nitrogen at this thickness is 0.87. It is apparent that processing in ambient air leads to a decrease in J_{sc} of the solar cell, which is consistent with the lower absorption coefficient and decreased PL intensity found, from optical investigation studies as well as with results from literature [138].

The EQE spectra of the solar cells (shown in figure 6.5) were measured to gain more information on the spectral distribution of the photocurrent. A slight blue shift of the range related to the P3HT (between 450 and 600 nm) and a visible decrease in the shoulder at 600 nm are seen when processing the active layer in air. This reduction, observed already in the absorption of the P3HT (figure 6.1), is a sign of reduced ordering, probably due to disruption of the polymer chains by the oxygen. In fact, it has been shown that the exposure of

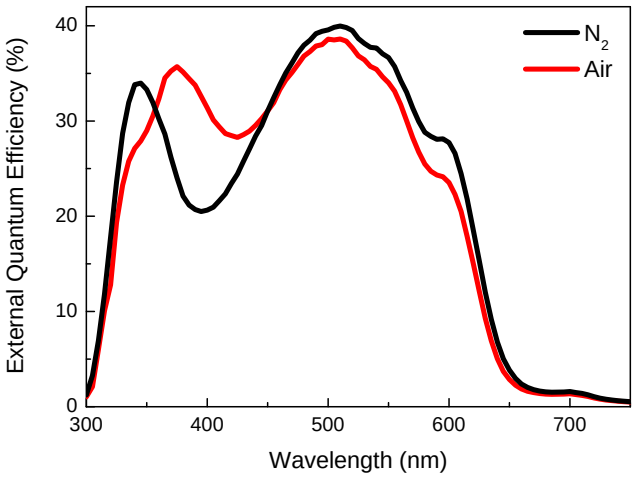

Figure 6.5: EQE spectra of the P3HT:PCBM solar cells processed in nitrogen (black) and in ambient air (red)

P3HT to light and oxygen leads to the destruction of the π-conjugated system in both solutions [146] and thin films [147, 148, 149]. The EQE spectrum of the cell prepared in air differs also in the range 300-400 nm where the fullerene PCBM absorbs. In particular, the PCBM related peak red shifts and broadens. This could be a sign that a competing process between the fullerene and oxygen occurs. Competition for the electron transfer between the oxygen incorporated in the active layer during the preparation and the PCBM could lead to a decrease of mobile electrons in the fullerene phase because of trapping by the oxygen, while increasing the hole density in the polymer phase. To summarize, the integrated EQE also decreases when the active layer is processed in ambient air.

The JV characteristics of the solar cells are shown in figure 6.6. As predicted by the optical modeling, the devices demonstrate a lower photocurrent when the blend was processed in air. No significant change in V_{oc} and FF is observed. The lower J_{sc} can be again attributed to a decrease in the density of mobile electrons in the blend upon trapping from molecular oxygen. The ratio of J_{sc} in air and in nitrogen is 0.81, as well as the ratio of the power conversion efficiency. The following relation holds

$$\frac{{PL_{area}}^{Air}}{{PL_{area}}^{N_2}} \cong \frac{{J_{scmax}}^{Air}}{{J_{scmax}}^{N_2}} \cong \frac{J_{sc}^{Air}}{J_{sc}^{N_2}} \cong \frac{\eta^{Air}}{\eta^{N_2}}, \tag{6.1}$$

which proves the consistency of the optical and photophysical findings with the devices. Lower and blue shifted absorption, PL quenching, and lower device

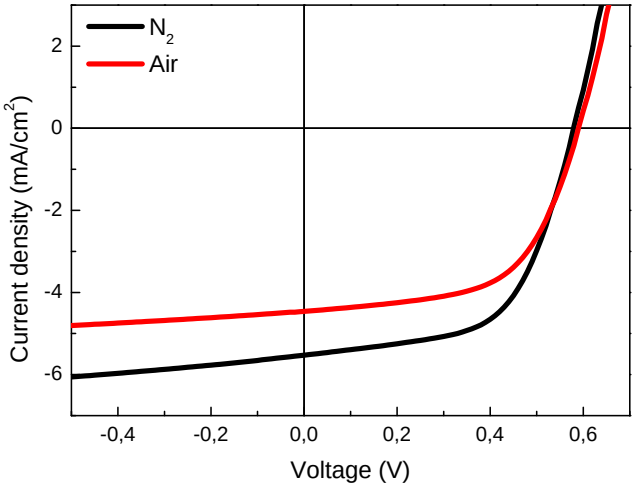

Figure 6.6: JV characteristics of the P3HT:PCBM solar cells processed in nitrogen (black) and in ambient air (red)

performance were also observed for cells prepared using purposely aged solutions [150]. In that case, the decrease in the solar cell performance is more dramatic and leads to significant drops also in FF and V_{oc}. Here, V_{oc} (580 mV for both cells) is not affected as well as FF (58.60% for the sample in nitrogen and 58.33% for the one in air), demonstrating that the oxygen/humidity incorporation in the active layer is not a limiting factor for the interface with the electrodes. On the other hand, this could also mean that the oxygen and water incorporation during processing does not detrimentally affect the surface of the layers, but is more likely to penetrate the bulk and act at the molecular level.

To summarize, the optoelectronic properties of P3HT and P3HT:PCBM layers are extremely sensitive to the atmosphere used for device processing. These results are significant when considering industrial processing conditions for preparing polymer:fullerene solar cells.

6.2 Effect of oxygen and light exposure

While it is hard to evaluate the effect of humidity on the optoelectronic properties of the blend, experiments that aim to understand the effect of oxygen are more feasible. Molecular oxygen is known to be an efficient luminescence quencher [139]. It has been shown that it causes reversible and irreversible detrimental effects to the performance of optoelectronic devices based on conjugated polymers

[138, 151, 152]. In P3HT based devices, the recovery of the initial luminescence is achieved by annealing the samples [153]. The irreversible component leads to a complete bleaching of the active layer and depends on the light intensity in presence of oxygen [153, 154].

The degradation is more critical when the oxygen exposure is coupled with light irradiation. In fact, both P3HT:PCBM layers and devices are almost not affected when exposing them to oxygen in the dark.

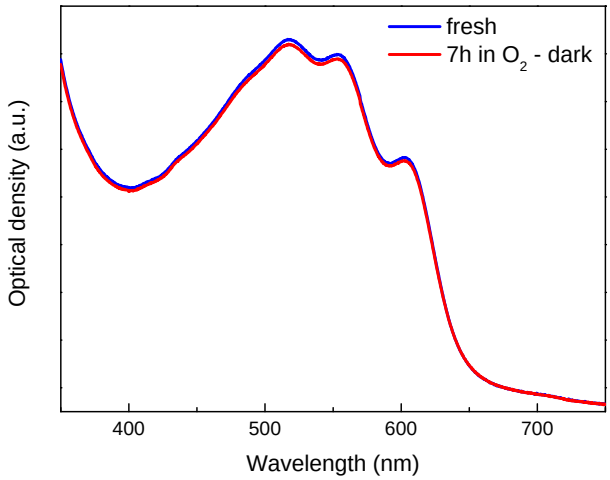

Figure 6.7: Optical density versus wavelength of P3HT:PCBM films before and after oxygen exposure in the dark

Figures 6.7 and 6.8 show, respectively, the optical density and the IV dark characteristic of a P3HT:PCBM solar cell before and after oxygen exposure in the dark. It is clear that, even after several hours, the optical properties are not changed. For the device, no changes take place after exposure of more than one hour.

In the following, the effect of oxygen induced irreversible photodegradation will be investigated. The samples were received from Konarka Technologies GmbH Nürnberg. Details of the preparation as well as the degradation procedure can be found in section 2.4.

6.2.1 Irreversible degradation studied combining PL and PIA spectroscopy

The effect of light induced degradation in the presence of oxygen in thin films of P3HT:PCBM is here studied by combining steady-state PL and PIA

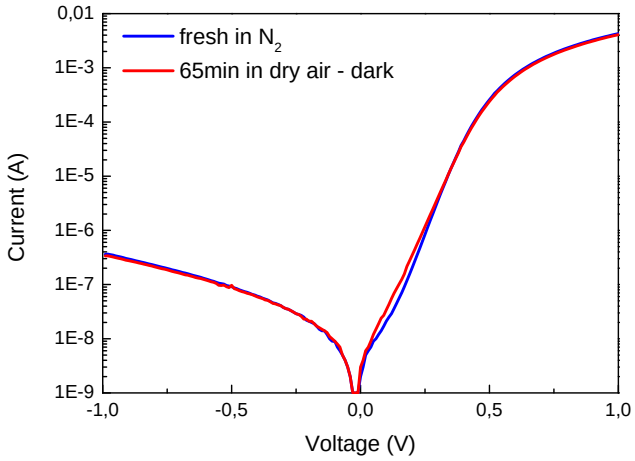

Figure 6.8: IV dark characteristics of P3HT:PCBM solar cells before and after oxygen exposure in the dark

spectroscopy. Figure 6.9 shows the absorbance spectra of the blends after degradation. The P3HT absorption band visibly decreases with increased exposure time and the decrease is independent of the wavelength. According to [155], the exposure time used here (shown in the inset in figure 6.9) is low enough to avoid effects on the morphology of the blends.

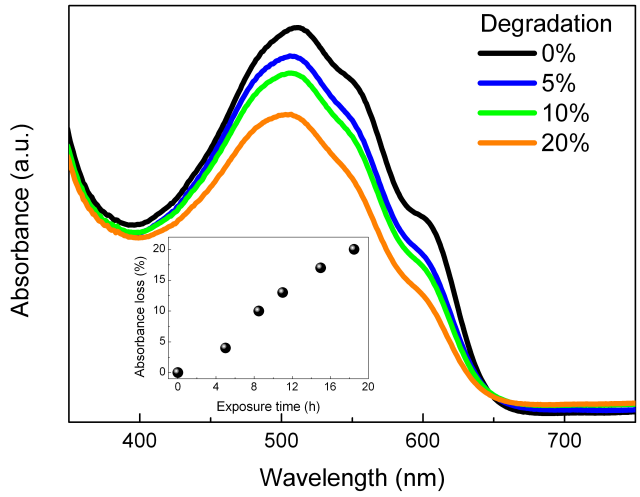

Figure 6.9: Absorbance spectra of the P3HT:PCBM blends degraded under light and synthetic air. The relative absorbance loss and the corresponding exposure time are reported in the inset [adapted from [156], measurement done by F. Deschler at the Ludwig-Maximilians-Universität, München]

Figure 6.10 shows the PL spectra of the degraded blends. It is apparent that

a longer exposure time to oxygen and light results in enhanced PL quenching. To get more information, the ratio between the PL of the fresh sample (PL_0) and the ones of the degraded samples is reported in figure 6.11 in a Stern-Volmer plot. From steady-state measurements, the quasi-linear behavior observed can be assigned to either collisional or static quenching [22].

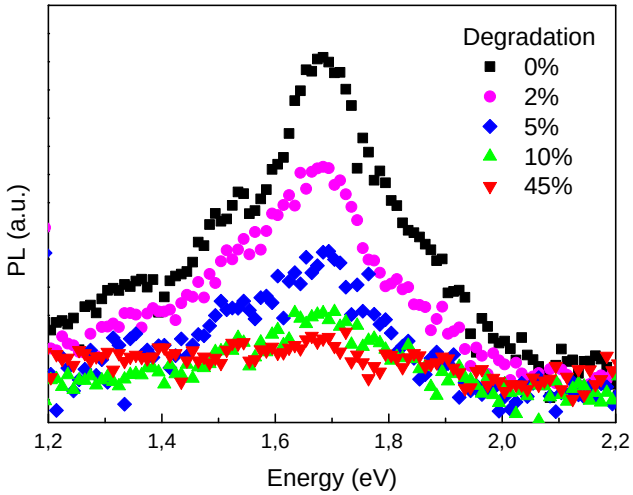

Figure 6.10: PL spectra of the P3HT:PCBM blends degraded under light in a synthetic air environment

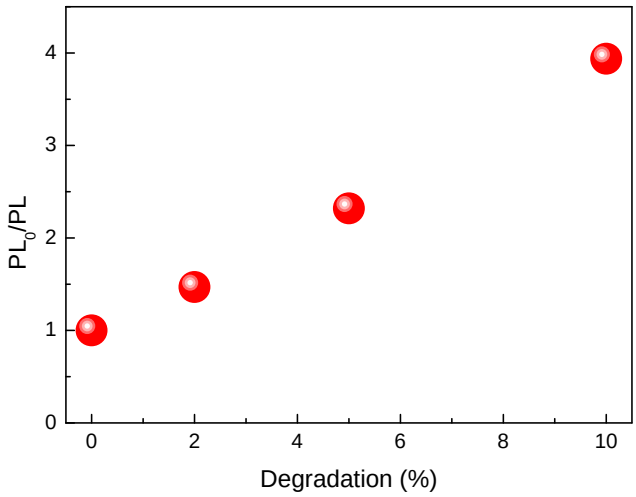

Figure 6.11: Stern-Volmer plot of the emission of the samples versus the degradation

This means that excitons diffusing in the polymer domains encounter quenching sites, whose number increases approximately linearly with the observed ab-

sorbance loss. Therefore, the blends exposed for longer time to the combination of light and oxygen have a higher concentration of quenching sites related to species generated during the photo-oxidation process [156]. Part of the excitons could also be quenched through ground state charge transfer complexes formed with oxygen or radicals originating from degradation products [157]. Both mechanisms represent a loss channel for exciton separation.

Although the PL data already provide valuable information on the light induced degradation of the films, they do not allow for monitoring the charge transfer process, which is of fundamental importance in a photovoltaic blend. For this reason, steady-state PIA on the same samples was also performed.

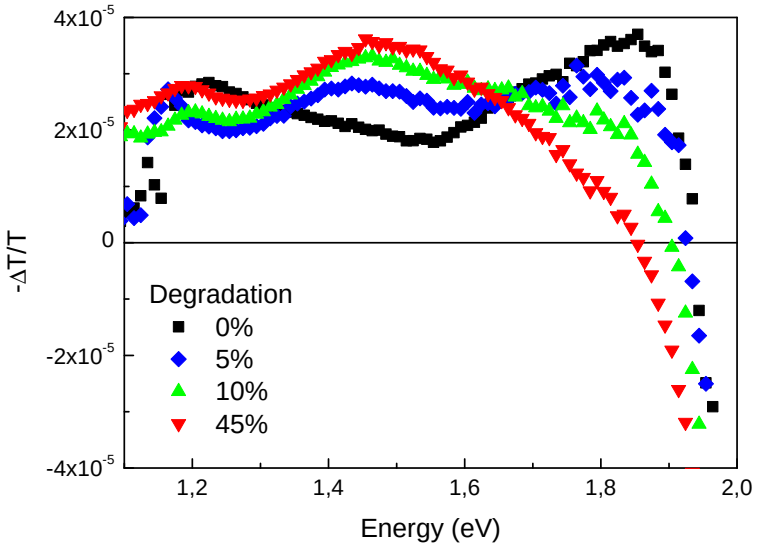

Figure 6.12: PIA spectra of the P3HT:PCBM blends degraded under light in a synthetic air environment

Figure 6.12 shows the PIA spectra of the degraded blends. Two features at 1.21 eV and 1.85 eV dominate the spectrum of the fresh sample (black squares). The peak at lower energy (1.21 eV) is assigned to localized intrachain polaron species, while the one at higher energy (1.85 eV) refers to delocalized interchain polarons and is related to the order in the films [144]. In fact, self-organization of the P3HT chains results in lamellae structures [158], in which strong interchain interaction due to the short interlayer distance leads to delocalization of the charge carrier. This is particularly pronounced in rr-P3HT and is the reason for the high mobility.

In the degraded blends, the localized polaron peak is not significantly af-

fected, while the one related to the delocalized polaron species visibly decreases with increasing exposure time. This is a sign that the combination of light and oxygen destroyes the ordering in rr-P3HT:PCBM blends. Moreover, a new broad photoinduced absorption band between 1.35 and 1.65 eV, that is not visible in the fresh sample, appears. A feature at these energies is usually not observed in rr-P3HT, but is characteristic of regio-random (ra) P3HT [144] and is assigned to a triplet transition which is not expected in rr-P3HT due to the higher ordering conformation of the polymer. The appearance of a triplet excitation could, therefore, be regarded as distroyed ordering in the films due to the interaction of light and oxygen with the polymer itself. Moreover, light induced degradation due to oxygen may disrupt the conjugation of the polymer or create degradation products where intersystem crossing is enhanced [159]. In the blend with PCBM, the enhancement of the long lived excitation population is obviously a loss path that hinders efficient charge separation.

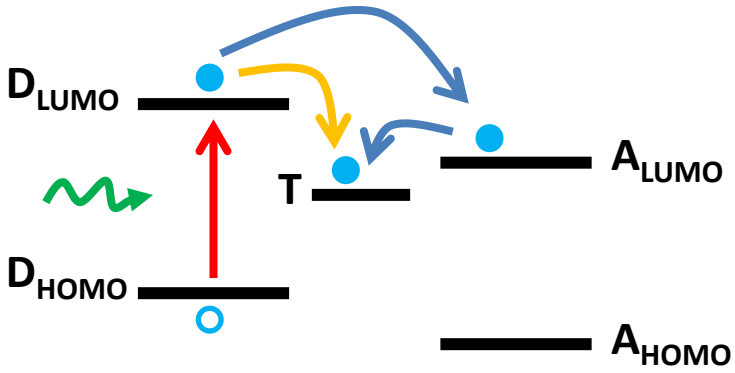

Figure 6.13: Possible loss mechanism due to oxygen in the blend

Figure 6.13 illustrates the possible competing processes that withstand charge transfer between P3HT and PCBM. In particular, intersystem crossing to the triplet manifold enhanced by oxygen is indicated by the orange arrow as a possible loss mechanism. Another scenario is represented by the blue arrows, where back transfer of the separated charges from the acceptor to the triplet can occur. Both processes are loss mechanisms interfering with efficient photovoltaic action in the polymer:fullerene blend.

6.3 Summary

It has been demonstrated that investigation of the degradation mechanism of the active layer is of fundamental importance to understand the degradation of the complete solar cells and to enable the design of more robust conjugated polymers as well as device structures. Furthermore, it is shown that PIA spectroscopy is a valuable tool which gives unique insights into the population dynamics of excitons and polarons and enables to study the effect of degradation on the optoelectronic properties of conjugated polymers.

Chapter 7

Conclusions

Different methods to enhance the performance of polymer:fullerene bulk heterojunction solar cells were shown by using two different kinds of donor polymers. Both fundamental and application-oriented aspects were investigated.

For the low bandgap copolymer PCPDTBT, molecular doping with F4-TCNQ was proposed as an effective method to control the electronic properties. Improvements of the charge transport by increasing the hole mobility in both the neat copolymer and in the blend with PCBM are demonstrated. In the blend with PCBM, in particular, increased polaron density and enhancement of the photovoltaic performance are achieved without a significant change in the morphology. This means that the improvements are due to the modification of the electronic properties of the copolymer upon doping.

For the semicrystalline P3HT polymer, a route to fine tuning of the morphology via combination of solvents with different boiling points has been proposed. Enhanced phase segregation between the polymer and fullerene phases and higher ordering of the polymer phase is induced by the introduction of a high boiling point co-solvent and results in higher photocurrents.

The influence of the device architecture was also addressed. In this direction, ITO and PEDOT:PSS free solar cells in the inverted structure were fabricated and optimized. ZnO:Al was used as the TCO, and it was demonstrated that it is a valid alternative to ITO. From the point of view of the device stability and manufacturing, the inverted architecture is more attractive, because water-based transport layers and low work function metals are avoided without sacrificing the

device efficiency.

In the last part, the degradation issue in P3HT:PCBM was addressed. The improved understanding of the degradation mechanisms of a model polymer like P3HT is essential in increasing the intrinsic stability of new conjugated polymers for photovoltaic applications. Here it was demonstrated, by using steady-state PIA spectroscopy combined with PL, that the loss of photocurrent and performance generally observed upon degradation results from the appearance of a long-lived population of triplet excitons.

Bibliography

[1] R.H. Friend. *Pure and Applied Chemistry*, 73:425, 2001. [cited at p. 1]

[2] R. Hoffmann, C. Janiak, and C. Kollmar. *Macromolecules*, 24:3725, 1991. [cited at p. 1]

[3] W. Barford. *Electronic and Optical Properties of Conjugated Polymers*. Oxford University Press, Oxford, 2009. [cited at p. 2, 7]

[4] S. Baranovski. *Charge Transport in Disordered Solids with Applications in Electronics*. Wiley, UK, 2006. [cited at p. 2]

[5] S.C. Graham, D.D.C. Bradley, R.H. Friend, and C. Spangler. *Synthetic Metals*, 41:1277, 1991. [cited at p. 2]

[6] N.S. Sariciftci. *Primary Photoexcitations in Conjugated Polymers: Molecular Exciton versus Semiconductor Band Model*. World Scientific, Singapore, 1998. [cited at p. 2]

[7] R. Loudon. *American Journal of Physics*, 27:649, 1959. [cited at p. 2]

[8] K. Pakbaz, C.H. Lee, A.J. Heeger, T.W. Hagler, and D. McBranch. *Synthetic Metals*, 64:295, 1994. [cited at p. 2]

[9] D. Chirvase, Z. Chiguvare, M. Knipper, J. Parisi, V. Dyakonov, and J.C. Hummelen. *Journal of Applied Physics*, 93:3376, 2003. [cited at p. 2]

[10] S.M. Sze and K.K. Ng. *Physics of Semiconductor Devices*. Wiley, New York, 2007. [cited at p. 2]

[11] D. Fichou. *Journal of Materials Chemistry*, 10:571, 2000. [cited at p. 2]

[12] G. Hadziioannou and P.F. van Putten. *Semiconducting Polymers*. Wiley-VCH, Weinheim, 2000. [cited at p. 2]

[13] M. Schwoerer and H.C. Wolf. *Organic Molecular Solids*. Wiley-VCH, Weinheim, 2005. [cited at p. 2]

[14] G. Dennler, M. C. Scharber, and C. J. Brabec. *Advanced Materials*, 21:1323, 2009. [cited at p. 2, 11]

[15] R. Gaudiana and C.J. Brabec. *Nature Photonics*, 2:287, 2008. [cited at p. 2, 11]

[16] D.E. Markov, E. Amsterdam, P.W.M. Blom, A.B. Sieval, and J.C. Hummelen. *Journal of Physical Chemistry A*, 109:5266, 2005. [cited at p. 2]

[17] G.A. Chamberlain. *Solar Cells*, 8:47, 1983. [cited at p. 2]

[18] P. Bhattacharya. *Semiconductor Optoelectronic Devices*. Prentice Hall, New Jersey, 1997. [cited at p. 3]

[19] G. Yu, J. Gao, J. C. Hummelen, F. Wudl, and A. J. Heeger. *Science*, 270:1789, 1995. [cited at p. 3, 8]

[20] C.J. Brabec, S.E. Shaheen, C. Winder, N.S. Sariciftci, and P. Denk. *Applied Physics Letters*, 80:1288, 2002. [cited at p. 4]

[21] N.S. Sariciftci, L. Smilowitz, A.J. Heeger, and F. Wudl. *Science*, 258:1474, 1992. [cited at p. 5, 7]

[22] J.R. Lakowicz. *Principles of Fluorescence Spectroscopy*. Springer, New York, 2006. [cited at p. 5, 6, 27, 65]

[23] C.J. Brabec, G. Zerza, G. Cerullo, S. De Silvestri, S. Luzzati, J.C. Hummelen, and N.S. Sariciftci. *Chemical Physics Letters*, 340:232, 2001. [cited at p. 7]

[24] I.W. Hwang, D. Moses, and A.J. Heeger. *Journal of Physical Chemistry C*, 112:4350, 2008. [cited at p. 7]

[25] T. Förster. *Annalen der Physik*, 437:55, 1948. [cited at p. 7]

[26] C. Deibel and V. Dyakonov. *Reports on Progress in Physics*, 73:096401, 2010. [cited at p. 7, 9]

[27] Y.W. Soon, T.M. Clarke, W. Zhang, T. Agostinelli, J. Kirkpatrick, C. Dyer-Smith, I. McCulloch, J. Nelson, and J.R. Durrant. *Chemical Science*, 2:1111, 2011. [cited at p. 7]

[28] C.W. Tang. *Applied Physics Letters*, 48:183, 1986. [cited at p. 8]

[29] M.A. Green, K. Emery, Y. Hishikawa, and W. Warta. *Progress in Photovoltaics: Research and Applications*, 19:84, 2011. [cited at p. 8]

[30] Y. Liang, Z. Xu, J. Xia, S.T. Tsai, Y. Wu, and L. Yu G. Li, C. Ray. *Advanced Materials*, 22:E135, 2010. [cited at p. 8]

[31] C.J. Brabec, V. Dyakonov, J. Parisi, and N.S. Sariciftci. *Organic Photovoltaics: Concepts and Realization*. Springer, Berlin, 2003. [cited at p. 8, 17]

[32] L.M. Chen, Z. Hong, G. Li, and Y. Yang. *Advanced Materials*, 21:1434, 2009. [cited at p. 9, 40, 45]

[33] J.K.J. van Duren, X.N. Yang, J. Loos, C.W.T. Bulle-Lieuwma, A.B. Sieval, J.C. Hummelen, and R.A.J. Janssen. *Advanced Functional Materials*, 14:425, 2004. [cited at p. 9]

[34] S.E. Shaheen, C.J. Brabec, N.S. Sariciftci, F. Padinger, T. Fromherz, and J. Hummelen. *Applied Physics Letters*, 78:841, 2001. [cited at p. 9]

[35] H. Hoppe, T. Glatzel, M. Niggemann, W. Schwinger, F. Schaeffler, A. Hinsch, M.Ch. Lux-Steiner, and N.S. Sariciftci. *Thin Solid Films*, 511:587, 2006. [cited at p. 9]

[36] H.F. Padinger, R. Rittberger, and N.S. Sariciftci. *Advanced Functional Materials*, 13:1, 2003. [cited at p. 9]

[37] Y. Kim, S. Cook, S.M. Tuladhar, S.A. Choulis, J. Nelson, J.R. Durrant, D.D.C. Bradley, M. Giles, I. McCulloch, C.S. Ha, and M. Ree. *Nature Materials*, 5:197, 2006. [cited at p. 9]

[38] F.C. Chen, H.C. Tseng, and C.J. Ko. *Applied Physics Letters*, 92:103316, 2008. [cited at p. 9]

[39] C.V. Hoven, X.D. Dang, R.C. Coffin, J. Peet, T.Q. Nguyen, and G.C. Bazan. *Advanced Materials*, 22:E63, 2010. [cited at p. 9]

[40] J. Peet, C. Soci, R.C. Coffin, T.Q. Nguyen, A. Mikhailovsky, D. Moses, and G.C. Bazan. *Applied Physics Letters*, 89:252105, 2006. [cited at p. 9]

[41] J. Peet, J.Y. Kim, N.E. Coates, W.L. Ma, D. Moses, A.J. Heeger, and G.C. Bazan. *Nature Materials*, 6:497, 2007. [cited at p. 9, 25]

[42] J.K. Lee, W.L. Ma, C.J. Brabec, J. Yuen, J.S. Moon, J.Y. Kim, K. Lee, G.C. Bazan, and A.J. Heeger. *Journal of the American Chemical Society*, 130:3619, 2008. [cited at p. 9]

[43] A. Pivrikas, P. Stadler, H. Neugebauer, and N.S. Sariciftci. *Organic Electronics*, 9:775, 2008. [cited at p. 9]

[44] L. Li, H. Tang, H. Wu, G. Lu, and X. Yang. *Organic Electronics*, 10:1334, 2009. [cited at p. 9, 35]

[45] H. Hoppe and N.S. Sariciftci. *Journal of Materials Research*, 19:1924, 2004. [cited at p. 10]

[46] A.J. Heeger, W. Ma, X. Gong, C. Yang, and K. Lee. *Advanced Functional Materials*, 15:1617, 2005. [cited at p. 10]

[47] C.J. Brabec. *Solar Energy Materials and Solar Cells*, 83:273, 2004. [cited at p. 10]

[48] C.J. Brabec, J.A. Hauch, P. Schilinsky, and C. Waldauf. *MRS Bulletin*, 30:50, 2005. [cited at p. 10]

[49] F.C. Krebs. *Refocus*, 6:38, 2005. [cited at p. 10]

[50] M. Jørgensen, K. Norrman, and F. C. Krebs. *Solar Energy Materials and Solar Cells*, 92:686, 2008. [cited at p. 11, 55, 56]

[51] J.Y. Kim, K. Lee, N.E. Coates, D. Moses, T.Q. Nguyen, M. Dante, and A.J. Heeger. *Science*, 317:222, 2007. [cited at p. 11]

[52] E. von Hauff, J. Parisi, and V. Dyakonov. *Thin Solid Films*, 511-512:506, 2006. [cited at p. 18]

[53] S. Bange, M. Schubert, and D. Neher. *Physical Review B*, 81:035209, 2010. [cited at p. 19]

[54] C.K. Chiang, C.R. Fincher, Y.W. Park, A.J. Heeger, H. Shirakawa, E.J. Louis, S.C. Gau, and A.G. MacDiarmid. *Physical Review Letters*, 39:1098, 1977. [cited at p. 23]

[55] J. Blochwitz, M. Pfeiffer, T. Fritz, and K. Leo. *Applied Physics Letters*, 73:729, 1998. [cited at p. 23, 25]

[56] C. Falkenberg, C. Uhrich, S. Olthof, B. Maennig, M.K. Riede, and K. Leo. *Journal of Applied Physics*, 104:034506, 2008. [cited at p. 23]

[57] C. K. Chan, W. Zhao, A. Kahn, and I.G. Hill. *Applied Physics Letters*, 94:203306, 2009. [cited at p. 23]

[58] W.Y. Gao and A. Kahn. *Journal of Applied Physics*, 94:359, 2003. [cited at p. 23]

[59] Y. Zhang, B. de Boer, and P.W.M. Blom. *Advanced Functional Materials*, 19:1901, 2009. [cited at p. 23, 25, 31]

[60] Y.A. Zhang and P.W.M. Blom. *Applied Physics Letters*, 97:083303, 2010. [cited at p. 23]

[61] C. Tanase, E.J. Meijer, P.W.M. Blom, and D.M. de Leeuw. *Physical Review Letters*, 91:216601, 2003. [cited at p. 23, 25]

[62] H.Y. Chen, J.H. Hou, S.Q. Zhang, Y.Y. Liang, G.W. Yang, Y. Yang, L.P. Yu, Y. Wu, and G. Li. *Nature Photonics*, 3:649, 2009. [cited at p. 24]

[63] A. Dhanabalan, J.K.J. van Duren, P.A. van Hal, J.L.J. van Dongen, and R.A.J. Janssen. *Advanced Functional Materials*, 11:255, 2001. [cited at p. 24]

[64] M. Svensson, F. Zhang, O. Inganäs, and M.R. Andersson. *Synthetic Metals*, 135:137, 2003. [cited at p. 24]

[65] N. Blouin, A. Michaud, and M. Leclerc. *Advanced Materials*, 19:2295, 2007. [cited at p. 24]

[66] Z. Zhu, D. Waller, R. Gaudiana, M. Morana, D. Mühlbacher, M. Scharber, and C.J. Brabec. *Macromolecules*, 40:1981, 2007. [cited at p. 24, 49]

[67] D. Mühlbacher, M. Scharber, M. Morana, Z.G. Zhu, D. Waller, R. Gaudiana, and C.J. Brabec. *Advanced Materials*, 18:2884, 2006. [cited at p. 25]

[68] M. Lenes, M. Morana, C.J. Brabec, and P.W.M. Blom. *Advanced Functional Materials*, 19:1106, 2009. [cited at p. 25]

[69] G.M. Rangger, O.T. Hofmann, L. Romaner, G. Heimel, B. Bröker, R.P. Blum, R.L. Johnson, N. Koch, and E. Zojer. *Physical Review B*, 79:165306, 2009. [cited at p. 25]

[70] W.Y. Gao and A. Kahn. *Applied Physics Letters*, 79:4040, 2001. [cited at p. 25]

[71] W. Chen, S. Chen, D.C. Qi, X.Y. Gao, and A.T.S. Wee. *Journal of the American Chemical Society*, 129:10418, 2007. [cited at p. 25]

[72] F. Deschler, E. Da Como, T. Limmer, R. Trautz, T. Godde, M. Bayer, E. von Hauff, S. Yilmaz, S. Allard, U. Scherf, and J. Feldmann. *Physical Review Letters*, 107:127402, 2011. [cited at p. 26, 30, 33]

[73] A.V. Tunc, A. De Sio, D. Riedel, F. Deschler, E. Da Como, J. Parisi, and E. von Hauff. *Organic Electronics*, 13:290, 2012. [cited at p. 27]

[74] L. Ma, W.H. Lee, Y.D. Park, J.S. Kim, H.S. Lee, and K. Choa. *Applied Physics Letters*, 92:063310, 2008. [cited at p. 27]

[75] M. Morana, M. Wegscheider, A. Bonanni, N. Kopidakis, S. Shaheen, M. Scharber, Z. Zhu, D. Waller, R. Gaudiana, and C.J. Brabec. *Advanced Functional Materials*, 18:1757, 2008. [cited at p. 28]

[76] T. Clarke, A. Ballantyne, F. Jamieson, C.J. Brabec, J. Nelson, and J. Durrant. *Chemical Communications*, 1:89, 2009. [cited at p. 28]

[77] C. Melzer, E.J. Koop, V.D. Mihailetchi, and P.W.M. Blom. *Advanced Functional Materials*, 14:865, 2004. [cited at p. 29]

[78] D. Di Nuzzo, A. Aguirre, M. Shahid, V.S. Gevaerts, S.C.J. Meskers, and R.A.J. Janssen. *Advanced Materials*, 22:4321, 2010. [cited at p. 29]

[79] K. Vandewal, K. Tvingstedt, A. Gadisa, O. Inganäs, and J.V. Manca. *Nature Materials*, 8:904, 2009. [cited at p. 33]

[80] V. Shrotriya, J. Ouyang, R.J. Tseng G. Li, and Y. Yang. *Chemical Physics Letters*, 411:138, 2005. [cited at p. 35]

[81] P.J. Brown, D.S. Thomas, A. Köhler, J.S. Wilson, J.S. Kim, C.M. Ramsdale, H. Sirringhaus, and R.H. Friend. *Physical Review B*, 67:064203, 2003. [cited at p. 36]

[82] A. Zen, J. Pflaum, S. Hirschmann, W. Zhuang, F. Jaiser, U. Asawapirom, J.P. Rabe, U. Scherf, and D. Neher. *Advanced Functional Materials*, 14:757, 2004. [cited at p. 36]

[83] M. Johnsen, M.J. Paterson, J. Arnbjerg, O. Christiansen, C.B. Nielsen, M. Jørgensen, and P.R. Ogilby. *Physical Chemistry Chemical Physics*, 10:1177, 2008. [cited at p. 36]

[84] H. Hoppe, N. Arnold, D. Meissner, and N. S. Sariciftci. *Thin Solid Films*, 451-452:589, 2004. [cited at p. 36]

[85] J. Gilot, I. Barbu, M.M. Wienk, and R.A.J. Janssen. *Applied Physics Letters*, 91:113520, 2007. [cited at p. 36, 51]

[86] R. Blanc, R. Rivoira, and P. Rouard. *Comptes Rendus de l'Académie des Sciences*, B264:634, 1967. [cited at p. 37]

[87] R. Blanc, R. Rivoira, and P. Rouard. *Comptes Rendus de l'Académie des Sciences*, B265:1044, 1967. [cited at p. 37]

[88] G. Hass and L. Hadley. *Optical Constants of Metals*. In D.E. Gray, editor, *American Institute of Physics Handbook*, page 6.124. McGraw Hill, New York, 1972. [cited at p. 37]

[89] T.F. Coleman and Y. Li. *Mathematical Programming*, 67:189, 1994. [cited at p. 38]

[90] T.F. Coleman and Y. Li. *SIAM Journal on Optimization*, 6:418, 1996. [cited at p. 38]

[91] O.S. Heavens. *Optical Properties of Thin Solid Films*. Dover, New York, 1991. [cited at p. 38]

[92] X.N. Yang, J. Loos, S.C. Veenstra, W.J.H. Verhees, M.M. Wienk, J.M. Kroon, M.A.J. Michels, and R.A.J. Janssen. *Nano Letters*, 5:579, 2005. [cited at p. 39, 43]

[93] M. Hallermann, I. Kriegel, E. Da Como, J.M. Berger, E. von Hauff, and J. Feldmann. *Advanced Functional Materials*, 19:3662, 2009. [cited at p. 39]

[94] G. Li, V. Shrotriya, J. Huang, Y. Yao, T. Moriarty, K. Emery, and Y. Yang. *Nature Materials*, 4:864, 2005. [cited at p. 40]

[95] Y. Yao, J. Hou, Z. Xu, G. Li, and Y. Yang. *Advanced Functional Materials*, 18:1783, 2008. [cited at p. 40]

[96] T. Glatzel, H. Hoppe, N.S. Sariciftci, M.Ch. Lux-Steiner, and M. Komiyama. *Japanese Journal of Applied Physics*, 44:5370, 2005. [cited at p. 40]

[97] A. De Sio, T. Madena, R. Huber, J. Parisi, S. Neyshtadt, F. Deschler, E. Da Como, S. Esposito, and E. von Hauff. *Solar Energy Materials and Solar Cells*, 95:3536, 2011. [cited at p. 40]

[98] K. Vandewal, A. Gadisa, W.D. Oosterbaan, S. Bertho, F. Banishoeib, I. Van Severen, L. Lutsen, T.J. Cleij, D. Vanderzande, and J.V. Manca. *Advanced Functional Materials*, 18:2064, 2008. [cited at p. 40, 42]

[99] M. Campoy-Quiles, T. Ferenczi, T. Agostinelli, P.G. Etchegoin, Y. Kim, T.D. Anthopoulos, P.N. Stavrinou, D.D.C. Bradley, and J. Nelson. *Nature Materials*, 7:158, 2008. [cited at p. 40, 45]

[100] S.S. Lee and Y.L. Loo. *Annual Reviews: Chemical and Biomolecular Engineering*, 1:59, 2010. [cited at p. 40]

[101] A.J. Mozer, G. Dennler, N.S. Sariciftci, M. Westerling, A. Pivrikas, R. Österbacka, and G. Juška. *Physical Review B*, 72:35217, 2005. [cited at p. 41]

[102] A. Pivrikas, N.S. Sariciftci, G. Juška, and R. Österbacka. *Progress in Photovoltaics: Research and Applications*, 15:677, 2007. [cited at p. 41]

[103] J. Lorrmann, B.H. Badada, O. Inganäs, V. Dyakonov, and C. Deibel. *Journal of Applied Physics*, 108:113705, 2010. [cited at p. 41]

[104] F. Zhang, K. G. Jespersen, C. Björström, M. Svensson, M. R. Andersson, V. Sundström, K. Magnusson, E. Moons, A. Yartsev, and O. Inganäs. *Advanced Functional Materials*, 16:667, 2006. [cited at p. 44]

[105] A. Tanaka, M. Hirata, Y. Kiyohara, M. Nakano, K. Omae, M. Shiratani, and K. Koga. *Thin Solid Films*, 518:2934, 2009. [cited at p. 45]

[106] K. Norrman and F.C. Krebs. *Progess in Photovoltaics: Research and Applications*, 15:697, 2007. [cited at p. 45]

[107] B. Tremolet de Villers, C.J. Tassone, S.H. Tolbert, and B.J. Schwarz. *Journal of Physical Chemistry C*, 113:18978, 2009. [cited at p. 45]

[108] M.Y. Song, K.J. Kim, and D.Y. Kim. *Solar Energy Materials and Solar Cells*, 85:31, 2005. [cited at p. 46]

[109] A. Watanabe and A. Kasuya. *Thin Solid Films*, 483:358, 2005. [cited at p. 46]

[110] G.B. Murdoch, S. Hinds, E.H. Sargent, S.W. Tsang, L. Mordoukhovski, and Z.H. Lub. *Applied Physics Letters*, 94:213301, 2009. [cited at p. 46]

[111] H.K. Park, J.W. Kang, S.I. Na, D.Y. Kim, and H.K. Kim. *Solar Energy Materials and Solar Cells*, 93:1994, 2009. [cited at p. 46]

[112] T. Minami, H. Sato, H. Nanto, and S. Takata. *Japanese Journal of Applied Physics*, 24:L781, 1985. [cited at p. 47]

[113] T. Minami, T. Yamamoto, and T. Miyata. *Thin Solid Films*, 366:63, 2000. [cited at p. 47]

[114] H.L. Hartnagel, A.L. Dawar, A.K. Jain, and C. Jagadish. *Semiconducting Transparent Thin Films*. Institute of Physics Publishing, Bristol, 1995. [cited at p. 47]

[115] M. Berginski, J. Hüpkes, M. Schulte, G. Schöpe, H. Stiebig, B. Rech, and M. Wuttig. *Journal of Applied Physics*, 101:074903, 2007. [cited at p. 47]

[116] M.A. Martínez, J. Herrero, and M.T. Gutiérrez. *Solar Energy Materials and Solar Cells*, 45:75, 1997. [cited at p. 47]

[117] H. Kim, A. Piqué, J.S. Horwitz, H. Murata, Z.H. Kafafi, C.M. Gilmore, and D.B. Chrisey. *Thin Solid Films*, 377-378:798, 2000. [cited at p. 47]

[118] J. Hu and R.G. Gordon. *Journal of Applied Physics*, 71:880, 1992. [cited at p. 47]

[119] C. Fournier, O. Bamiduro, H. Mustafa, R. Mundle, R.B. Konda, F. Williams, and A.K. Pradhan. *Semiconductor Science and Technology*, 23:085019, 2008. [cited at p. 47]

[120] K.J. Reynolds, J.A. Barker, N.C. Greenham, R.H. Friend, and G.L. Frey. *Journal of Applied Physics*, 92:7556, 2002. [cited at p. 49]

[121] V. Shrotriya, G. Li, Y. Yao, C.W. Chu, and Y. Yang. *Applied Physics Letters*, 88:073508, 2006. [cited at p. 49, 50]

[122] T. Yamanari, T. Taima, J. Sakai, J. Tsukamoto, and Y. Yoshida. *Japanese Journal of Applied Physics*, 49:01AC02, 2010. [cited at p. 49]

[123] E. Voroshazi, B. Verreet, A. Buri, R. Mller, D. Di Nuzzo, and P. Heremans. *Organic Electronics*, 12:736, 2011. [cited at p. 49]

[124] H.B. Michaelson. *Journal of Applied Physics*, 48:4729, 1977. [cited at p. 50]

[125] W.N. Hansen and K.B. Johnson. *Surface Science*, 316:373, 1994. [cited at p. 50]

[126] T.M. Brown, G.M. Lazzerini, L.J. Parrott, V. Bodrozic, L. Bürgi, and F. Cacialli. *Organic Electronics*, 12:623, 2011. [cited at p. 50]

[127] S. Scholz, Q. Huang, M. Thomschke, S. Olthof, P. Sebastian, K. Walzer, K. Leo, S. Oswald, C. Corten, and D. Kuckling. *Journal of Applied Physics*, 104:104502, 2008. [cited at p. 50]

[128] A.K.K. Kyaw, X.W. Sun, C.Y. Jiang, G.Q. Lo, D.W. Zhao, and D.L. Kwong. *Applied Physics Letters*, 93:221107, 2008. [cited at p. 50]

[129] D.W Zhao, S.T. Tan, L. Ke, P. Liu, A.K.K. Kyaw, X.W. Sun, G.Q. Lo, and D.L. Kwong. *Solar Energy Materials and Solar Cells*, 94:985, 2010. [cited at p. 51]

[130] J.Y. Kim, S.H. Kim, H.H. Lee, K. Lee, W. Ma, X. Gong, and A.J. Heeger. *Advanced Materials*, 18:572, 2006. [cited at p. 51]

[131] Y. Kanai, T. Matsushima, and H. Murata. *Thin Solid Films*, 518:537, 2009. [cited at p. 52]

[132] C.Y. Jiang, X.W. Sun, D.W. Zhao, A.K.K. Kyaw, and Y.N. Li. *Solar Energy Materials and Solar Cells*, 94:1618, 2010. [cited at p. 52, 57]

[133] R. Lessmann, Z. Hong, S. Scholz, B. Maennig, M.K. Riede, and K. Leo. *Organic Electronics*, 11:539, 2010. [cited at p. 55]

[134] C. Lin, E.Y. Lin, and F.Y. Tsai. *Advanced Functional Materials*, 20:834, 2010. [cited at p. 55]

[135] M.O. Reese, A.J. Morfa, M.S. White, N. Kopidakis, S.E. Shaheen, G. Rumbles, and D.S. Ginley. *Solar Energy Materials and Solar Cells*, 92:746, 2008. [cited at p. 55]

[136] T. Tromholt, E.A. Katz, B. Hirsch, A. Vossier, and F.C. Krebs. *Applied Physics Letters*, 96:073501, 2010. [cited at p. 55]

[137] R. Steim, S.A. Choulis, P. Schilinsky, U. Lemmer, and C.J. Brabec. *Applied Physics Letters*, 94:043304, 2009. [cited at p. 55]

[138] A. Seemann, T. Sauermann, C. Lungenschmied, O. Armbruster, S. Bauer, H.J. Egelhaaf, and J. Hauch. *Solar Energy*, 85:1238, 2011. [cited at p. 55, 60, 63]

[139] H. Kautsky. *Transactions of the Faraday Society*, 35:216, 1939. [cited at p. 57, 62]

[140] K. Kawano, R. Pacios, D. Poplavskyy, J. Nelson, D.D.C. Bradley, and J.R. Durrant. *Solar Energy Materials and Solar Cells*, 90:3520, 2006. [cited at p. 58]

[141] K. Norrman, S.A. Gevorgyan, and F.C. Krebs. *ACS Applied Materials and Interfaces*, 1:102, 2009. [cited at p. 58]

[142] R. Österbacka, C.P. An, X.M. Jiang, and Z.V. Vardeny. *Science*, 287:839, 2000. [cited at p. 58]

[143] T. Kobayashi, K. Kinoshita, T. Nagase, and H. Naito. *Physical Review B*, 83:035305, 2011. [cited at p. 58]

[144] O.J. Korovyanko, R. Österbacka, X.M. Jiang, Z.V. Vardeny, and R.A.J. Janssen. *Physical Review B*, 64:235122, 2001. [cited at p. 58, 66, 67]

[145] L. Smilowitz, N.S. Sariciftci, R. Wu, C. Gettinger, A.J. Heeger, and F. Wudl. *Physical Review B*, 47:13835, 1993. [cited at p. 59]

[146] M. Koch, R. Nicolaescu, and P.V. Kamat. *Journal of Physical Chemistry C*, 113:11507, 2009. [cited at p. 61]

[147] H. Hintz, H.J. Egelhaaf, H. Peisert, and T. Chassé. *Polymer Degradation and Stability*, 95:818, 2010. [cited at p. 61]

[148] N. Ljungqvist and T. Hjertberg. *Macromolecules*, 28:5993, 1995. [cited at p. 61]

[149] M.S.A. Abdou, F.P. Orfino, Z.W. Xie, M.J. Deen, and S. Holdcroft. *Advanced Materials*, 6:838, 1994. [cited at p. 61]

[150] Y.M. Chang, W.F. Su, and L. Wang. *Solar Energy Materials and Solar Cells*, 92:761, 2008. [cited at p. 62]

[151] H. Hintz, H.J. Egelhaaf, L. Lüer, J. Hauch, H. Peisert, and T. Chassé. *Chemistry of Materials*, 23:145, 2011. [cited at p. 63]

[152] A. Sperlich, H. Kraus, C. Deibel, H. Blok, J. Schmidt, and V. Dyakonov. *Journal of Physical Chemistry B*, 115:13513, 2011. [cited at p. 63]

[153] L. Lüer, H.J. Egelhaaf, D. Oelkrug, G. Cerullo, G. Lanzani, B.H. Huisman, and D. de Leeuw. *Organic Electronics*, 5:83, 2004. [cited at p. 63]

[154] M.S.A. Abdou and S. Holdcroft. *Canadian Journal of Chemistry*, 73:1893, 1995. [cited at p. 63]

[155] M.O. Reese, A.M. Nardes, B.L. Rupert, R.E. Larsen, D.C. Olson, M.T. Lloyd, S.E. Shaheen, D.S. Ginley, G. Rumbles, and N. Kopidakis. *Advanced Functional Materials*, 20:3476, 2010. [cited at p. 64]

[156] F. Deschler, A. De Sio, E. von Hauff, P. Kutka, T. Sauermann, H.J. Egelhaaf, J. Hauch, and E. Da Como. *Advanced Functional Materials*, 2012. accepted. [cited at p. 64, 66]

[157] H. Hintz, H. Peisert, H.J. Egelhaaf, and T. Chassé. *Journal of Physical Chemistry C*, 115:13373, 2011. [cited at p. 66]

[158] H. Sirringhaus, P.J. Brown, R.H. Friend, M.M. Nielsen, K. Bechgaard, B.M.W. Langeveld-Voss, A.J.H. Spiering, R.A.J. Janssen, E.W. Meijer, P. Herwig, and D.M. de Leeuw. *Nature*, 401:685, 1999. [cited at p. 66]

[159] N. Turro. *Modern Molecular Photochemistry*. University Science Books, Palo Alto, 1991. [cited at p. 67]

Acknowledgments

Many people have contributed to the realization of this work. I want to take the opportunity to thank them all:

- Prof Jürgen Parisi for giving me the possibility to work in his group, for his experience and fruitful discussions, and Prof Elizabeth von Hauff for the valuable guidance in the last three years, support and long enlightening discussions
- the staff of the Energy and Semiconductor Research Laboratory at the Uni Oldenburg, and in particular: Thomas Madena for the AFM and KPFM measurements; Ali Veysel Tunc for the OFET measurements; Ralph Huber for the CELIV measurements and for many helpful discussions; my long-time office collegues Marta Kruszynska and Bernhard Ecker; Florian Witt, Elena Selishcheva, Nikolay Radychev and Ivan Chernov for the nice time at and after work; Martin Knipper for introducing me to the PIA setup; Ulf Mikolajczak for valuable and experienced technical support; Janet Neerken for assistance during the EQE measurements; Matthias Macke for his always kind helpfulness with everything concerning the lab supplies; Elzbieta Chojnowski for taking care of all the administrative stuff
- the group of Dr Enrico Da Como at the Ludwig-Maximilians-Universität (München) for fruitful cooperation and discussion, specially Felix Deschler, Daniel Riedel and Shany Neyshtadt
- Kambulakwao Chakanga at the EWE Research Center Next Energy (Oldenburg) for the fabrication of the ZnO:Al substrates and the nice cooperation
- Salvatore Esposito at the ENEA Research Center in Portici (Italy) for the optical modeling
- financial support from the Bundesministerium für Bildung und Forschung through the "EOS Project" (03X3516E)
- Merck Chemicals ltd (UK) for supplying the P3HT and Dr Hans-Joachim Egelhaaf and its team at Konarka Technologies GmbH in Nürnberg for the PCPDTBT and part of the samples for the degradation experiments
- my parents and my sister in Italy for their support and confidence in me
- Max for warm encouragement, fruitful discussion and for bearing my moods.

Erklärung

Hiermit erkläre ich, dass ich diese Arbeit selbständig verfasst und nur die angegebenen Hilfsmittel benutzt habe.

Oldenburg, den 01.02.2012

Antonietta De Sio

Curriculum vitae

Antonietta De Sio

Date of Birth	June 17th, 1981
Place of Birth	Salerno, Italy
Gender	female
Nationality	Italian

Education

since 01.2009 **PhD candidate**,
Energy and Semiconductor Research Laboratory,
Carl von Ossietzky University of Oldenburg, Germany.
Research field: *Organic photovoltaics*

2000 - 2008 **Master's degree in Electronic Engineering**,
University of Salerno, Italy,
Specialization: Microelectronics.
Final thesis: *study of the optoelectronic properties of semiconducting polymers for application in organic solar cells*
Thesis performed at the ENEA Research Center in Portici, Italy

1995 - 2000 **High school**,
Institute Basilio Focaccia, Salerno, Italy.

Schools

13.09 - 20.09 2009 Quantsol Summer School 2009
Hirschegg, Austria

21.09 - 25.09 2008 1st European School on Spectroscopic Ellipsometry
Ostuni, Italy
Participation with scholarship from NanoCharM

07.08 - 29.09 2006 Summer Student Programme 2006
Hahn-Meitner-Institut Berlin, Germany
Topic: *optical, electrical and structural characterization of $CuInS_2$ absorber layers and solar cells*